NASA TECHNICAL NOTE

NASA TN D-6058

c. 1

NASA TN D-6058

WIND-TUNNEL INVESTIGATION OF A JET TRANSPORT AIRPLANE CONFIGURATION WITH HIGH THRUST-WEIGHT RATIO AND AN EXTERNAL-FLOW JET FLAP

by Lysle P. Parlett, Delma C. Freeman, Jr., and Charles C. Smith, Jr.

Langley Research Center
Hampton, Va. 23365

NATIONAL AERONAUTICS AND SPACE ADMINISTRATION • WASHINGTON, D. C. • NOVEMBER 1970

1. Report No.	2. Government Accession No.	
NASA TN D-6058		

4. Title and Subtitle	5. Report Date
WIND-TUNNEL INVESTIGATION OF A JET TRANSPORT AIRPLANE CONFIGURATION WITH HIGH THRUST-WEIGHT RATIO AND AN EXTERNAL-FLOW JET FLAP	November 1970
	6. Performing Organization Code
7. Author(s)	8. Performing Organization Report No.
Lysle P. Parlett, Delma C. Freeman, Jr., and Charles C. Smith, Jr.	L-7166
	10. Work Unit No.
9. Performing Organization Name and Address	721-01-11-06
NASA Langley Research Center Hampton, Va. 23365	11. Contract or Grant No.
	13. Type of Report and Period Covered
12. Sponsoring Agency Name and Address	Technical Note
National Aeronautics and Space Administration Washington, D.C. 20546	14. Sponsoring Agency Code

15. Supplementary Notes

16. Abstract

An investigation has been conducted in the Langley full-scale tunnel to determine the aerodynamic and stability and control characteristics of a jet transport configuration that has a high thrust-weight ratio and is equipped with an external-flow jet flap. The model is powered by four high-bypass-ratio turbofan engines.

Maximum lift coefficients of about 8 were measured for test conditions which simulated a jet transport configuration having a thrust-weight ratio of about 0.5. Longitudinal instability was encountered at high thrust coefficients because of adverse downwash variations in the vicinity of the tail. This problem was solved by raising the tail and moving it forward to a more favorable downwash field. The model was laterally and directionally stable under all power conditions. The moments associated with an engine failure were too large to be trimmed out by conventional aileron and rudder control; spoilers alone provided enough control to offset the engine-out rolling moments but the lift loss associated with the use of spoilers was severe.

17. Key Words (Suggested by Author(s))

External-flow jet flap
High lift
Stability and control
STOL

18. Distribution Statement

Unclassified – Unlimited

19. Security Classif. (of this report)	20. Security Classif. (of this page)	21. No. of Pages	22. Price*
Unclassified	Unclassified	74	$3.00

*For sale by the Clearinghouse for Federal Scientific and Technical Information
Springfield, Virginia 22151

WIND-TUNNEL INVESTIGATION OF A JET TRANSPORT AIRPLANE CONFIGURATION WITH HIGH THRUST-WEIGHT RATIO AND AN EXTERNAL-FLOW JET FLAP

By Lysle P. Parlett, Delma C. Freeman, Jr.,
and Charles C. Smith, Jr.
Langley Research Center

SUMMARY

An investigation has been conducted in the Langley full-scale tunnel to determine the aerodynamic and stability and control characteristics of a jet transport configuration that has a high thrust-weight ratio and is equipped with an external-flow jet flap. The model is powered by four high-bypass-ratio turbofan engines.

Maximum lift coefficients of about 8 were measured for test conditions which simulated a jet transport configuration having a thrust-weight ratio of about 0.5. Longitudinal instability was encountered at high thrust coefficients because of adverse downwash variations in the vicinity of the tail. This problem was solved by raising the tail and moving it forward to a more favorable downwash field. The model was laterally and directionally stable under all power conditions. The moments associated with an engine failure were too large to be trimmed out by conventional aileron and rudder control; spoilers alone provided enough control to offset the engine-out rolling moments but the lift loss associated with the use of spoilers was severe.

INTRODUCTION

Recent interest in the development of jet-powered STOL transport aircraft has led to serious consideration of the external-flow jet flap as a means of producing the high lift required for STOL operation. Early experimental work (refs. 1 to 3) demonstrated the feasibility of this concept for producing high lift, but interest in the idea decreased mainly because of the problems caused by heating of the aircraft structures. The more recent development of high-bypass turbofan engines with relatively cool exhaust has minimized this problem and made the concept much more feasible from structural considerations.

In the application of the jet-flap concept to STOL aircraft, consideration must be given to stability and control at very low speeds, particularly in terms of safe operation

with a critical engine inoperative. Very little experimental information of this type is available from which basic problem areas can be identified and from which effective design features can be established for practical hardware application. One recent experimental study (ref. 4) provided some information on the stability and control characteristics of a jet STOL aircraft equipped with a jet flap, but there is a need for much more experimental work of this type to provide more complete research information. For this reason, the present investigation was undertaken and, in order to expedite the testing, an existing model was used. Even though the model had been used in a previous study to simulate an aircraft with a fairly low thrust-weight ratio (see ref. 5), the configuration seemed desirable for simulation of an STOL transport with a high thrust-weight ratio for several reasons: (1) The model had a high wing to minimize adverse ground effects, (2) the wing was swept to help in spreading the jet exhaust over the flap, and (3) the horizontal tail was located high on the vertical tail to help in minimizing adverse downwash effects.

In the present investigation, tests were made over angle-of-attack and angle-of-sideslip ranges for several thrust coefficients and for several flap deflections. In addition, tests were made under various conditions of asymmetric thrust and asymmetric control deflections. Also, flow survey measurements were made in the vicinity of the horizontal tail to determine the downwash variation for a jet-flap configuration operating at very high lift coefficients.

SYMBOLS

The longitudinal data are referred to the stability-axis system and the lateral data are referred to the body-axis system. (See fig. 1.) The origin of the axes was at the center-of-gravity position (0.446 mean aerodynamic chord) shown in figure 2.

In order to facilitate international usage of the data presented, dimensional quantities are presented both in U.S. Customary Units and in the International System of Units (SI). Equivalent dimensions were determined by using the conversion factors given in reference 6.

b wing span, ft (m)

C_D drag coefficient, F_D/qS

C_L lift coefficient, F_L/qS

C_l rolling-moment coefficient, M_X/qSb

$C_{l_\beta} = \frac{\partial C_l}{\partial \beta}$, per deg

C_m pitching-moment coefficient, $M_Y/qS\bar{c}$

C_n yawing-moment coefficient, M_Z/qSb

$C_{n_\beta} = \frac{\partial C_n}{\partial \beta}$, per deg

C_Y side-force coefficient, F_Y/qS

$C_{Y_\beta} = \frac{\partial C_Y}{\partial \beta}$, per deg

C_μ engine gross-thrust coefficient, $\dot{m}V_E/qS$

c local wing chord, in. (cm)

$\bar{c}$ mean aerodynamic chord, in. (cm)

F_A axial force, positive rearward, lb (N)

F_D drag force, lb (N)

F_L lift force, lb (N)

F_N normal force, positive upward, lb (N)

F_X force along X-axis, positive forward, lb (N)

F_Y side force, positive to the right, lb (N)

i_t horizontal-tail incidence angle, deg

l tail length (measured from center of gravity to $\bar{c}/4$ of horizontal tail), in. (cm)

M_X rolling moment, ft-lb (m-N)

M_Y pitching moment, ft-lb (m-N)

M_Z	yawing moment, ft-lb (m-N)
$\dot{m}$	engine mass-flow rate, slugs/sec (kg/sec)
q	free-stream dynamic pressure, $\rho V^2/2$, lb/ft^2 (N/m^2)
r	radius of curvature, in. (cm)
S	wing area, ft^2 (m^2)
T	thrust, lb (N)
V	free-stream velocity, ft/sec (m/sec)
V_E	engine exit velocity, ft/sec (m/sec)
X,Y,Z	body reference axes
X_S,Y_S,Z_S	stability reference axes
z	tail height (measured from top of fuselage to horizontal tail), in. (cm)
α	angle of attack, deg
β	angle of sideslip, deg
δ_{aL}	deflection of left aileron, positive when trailing edge is down, deg
δ_{aR}	deflection of right aileron, positive when trailing edge is down, deg
δ_e	elevator deflection, positive when trailing edge is down, deg
δ_{f1}	deflection of forward segment of trailing-edge flap, deg
δ_{f2}	deflection of aft segment of trailing-edge flap, deg
$\left(\delta_{f1}/\delta_{f2}\right)_L$	deflection of left trailing-edge flap, deg
$\left(\delta_{f1}/\delta_{f2}\right)_R$	deflection of right trailing-edge flap, deg

δ_j jet deflection, deg

δ_r rudder deflection, positive when trailing edge is to the left, deg

ϵ downwash angle, deg

$1 - \frac{\partial \epsilon}{\partial \alpha}$ downwash factor

η flap turning efficiency, $\frac{\sqrt{F_A{}^2 + F_N{}^2}}{T}$

ρ air density, slugs/ft^3 (kg/m^3)

MODEL AND APPARATUS

The tests were made in the 30- by 60-foot (9.1- by 18.3-m) open-throat test section of the Langley full-scale tunnel with the model mounted about 10 feet (3.05 m) above the ground board. The model was so small in proportion to the test section that no wind-tunnel wall corrections were needed or applied. Normal corrections for flow angularity were applied.

The investigation was conducted on the four-engine, high-wing, jet-transport model illustrated by the three-view drawing of figure 2(a). The model was the same as that used in reference 5 except that the leading-edge slats were replaced with leading-edge flaps and the chord of the aft segment of the trailing-edge flaps was doubled. The dimensional characteristics of the model are given in table I. A detailed sketch of the flap assembly and engine-pylon arrangement is shown in figure 2(b). Details of the leading-edge flap configuration and the jet exhaust deflectors employed during the tests are presented in figures 2(c) and 2(d), respectively. A photograph of the model mounted for static force tests in the Langley full-scale tunnel is presented in figure 3.

To facilitate configuration changes and to insure accurate flap deflection angles, the wing of the model was designed with removable trailing edges. To convert the model from the clean configuration to each of the flap-deflected configurations, the clean trailing edges were replaced with trailing-edge flaps constructed with fixed gaps, overlaps, and deflection angles. The leading-edge flaps were designed so that they could be fastened to the wing leading edge at fixed positions when desired. Because of this arrangement, only the leading- and trailing-edge flap deflections shown in figure 2 could be achieved for the tests.

The model engines represented high-bypass-ratio turbofans and were installed at -3° incidence (referred to the X-axis) so that for the basic condition the jet exhaust

impinged directly on the trailing-edge flap system. In addition, in an attempt to achieve better spreading and to improve the turning efficiency of the system, several jet-exhaust deflectors (see fig. 2(d)) were tested and the most promising deflector was employed in most of the tests. The engine turbines were driven by compressed air and turned fans which produced the desired thrust.

All of the tests were made with an internal strain-gage balance and conventional sting which entered the rear of the fuselage.

TESTS AND PROCEDURES

In preparation for the tests, the engines were calibrated to determine gross thrust as a function of engine rotational speed in the static condition – at zero angle of attack with the thrust deflectors off. The tests were then run by setting the engine rotational speed to give the desired thrust and holding this speed constant through the ranges of angles of attack or sideslip.

Jet deflection angles and flap turning efficiency were determined from measurements of normal and axial forces made in the static thrust condition with flaps deflected. The static thrust used in computing turning efficiency was taken directly from the engine calibrations at the appropriate rotational speed.

During the wind-on tests various changes were made to the flap geometry or to control-surface deflections. Most tests were made for flap deflections of $\delta_{f1}/\delta_{f2} = 20^o/40^o$ and $\delta_{f1}/\delta_{f2} = 30^o/60^o$ for a range of C_μ from 0 to 3.5 and a range of angles of attack of -5^o to 30^o. Sideslip runs were made over a range of angles of sideslip from 15^o to -15^o. All wind-on tests were made at a free-stream dynamic pressure of about 3 lb/ft^2 (143.6 N/m^2), which corresponds to a velocity of 50 ft/sec (15.24 m/sec) and to a Reynolds number, based on the mean aerodynamic chord, of 0.35×10^6.

In addition to the force tests, a few flow survey measurements were made in the vicinity of the horizontal tail to determine the downwash variation with changes in thrust coefficient. The measurements were made with a simple vane of balsa wood which was free to pivot for alinement with the local flow. A potentiometer connected to the wooden vane produced electrical signals which indicated the flow angle.

RESULTS AND DISCUSSION

At the beginning of the test program, the wing of the model was equipped with the leading-edge slat arrangement described in reference 5. This slat arrangement was of conventional design and was effective at the low thrust-weight ratio of the jet-flap simulation of reference 5. It was found in the preliminary tests of the present investigation,

however, that at the higher thrust coefficients the leading-edge flow conditions with the original slat configuration were very unsatisfactory. Tuft studies, for example, showed that the wing leading edges were stalled at angles of attack of about 5°. It was found that lowering the slats and sealing the gaps between the slats and wing resulted in much better leading-edge flow conditions. Also, when the outboard slats were altered by increasing the chord and adding much more camber, it was possible to prevent the wing tips from stalling prematurely. With this leading-edge arrangement, identified as leading-edge flaps in the present paper, the wing stall could be delayed to angles of attack of about 20°.

Lift Characteristics

Wind off.- Because the jet-induced lift is highly dependent on the direction and velocity of the engine slipstream as it leaves the flap system, the flap system must be capable of turning the slipstream efficiently through large angles. In the present investigation a number of exhaust deflectors were tested to determine their effectiveness in spreading and turning the jet. The results of these tests are presented in figure 4, where the ratio of normal force to thrust F_N/T is plotted against the ratio of net axial force to thrust F_A/T. This figure shows that deflectors located on the bottom of the engine exhaust (see fig. 2(d)) gave the highest turning angle and highest efficiency. The lowest efficiencies were measured with deflectors off and with deflectors located in the middle of the jet or at the top of the jet. On the basis of these results, all the tests were made with deflector 1 since this deflector gave almost as much turning efficiency as the best (deflector 4) and was much smaller and therefore more practical.

Wind on.- Basic longitudinal data for the model in the tail-off configuration with trailing-edge flap deflections of $20^{\circ}/40^{\circ}$ and $30^{\circ}/60^{\circ}$ are presented in figures 5(a) and 5(b), respectively. The leading-edge flaps were extended for all test conditions. These figures show that the stall angle and the maximum lift coefficient increased with increasing thrust coefficient C_{μ} and that the effects of C_{μ} on the lift characteristics were more pronounced at the higher flap deflection. The higher flap deflection (fig. 5(b)) produced lift coefficients up to 8.3 (untrimmed) at a gross-thrust coefficient of 3.50. As would be expected, high lift coefficients are accompanied by large nose-down moments because of the rearward location of the flap loads.

The effectiveness of the jet-flap system of the present model is compared with that of the model of reference 1 in figure 6. The data of reference 1 do not necessarily represent ideal values, but they have been considered generally representative of the data to be expected from an efficient external-flow jet-flap system. The comparison is not exact because of some differences in jet angle and some differences in model and engine geometry; it does show, however, that the jet-flap system of the present model, which is more or less a conventional flap system converted to jet-flap operation, produced lift characteristics generally similar to those of the model of reference 1.

Longitudinal Stability and Trim With Symmetric Thrust

The longitudinal stability and trim characteristics of the model with tail on are plotted against angle of attack for various thrust levels and flap settings in figures 7 to 10. The lift characteristics of the horizontal tail alone are presented in figure 11, and data obtained in flow surveys in the vicinity of the horizontal tail are presented in figures 12 to 15.

The data of figure 7 show that the model in the cruise configuration was stable up through the stall with the center of gravity at $0.446\bar{c}$, which is farther rearward than is common for aircraft with more conventional horizontal tails. The data of figure 8 show that with flaps down and with the horizontal tail in the original location (see fig. 2(a)) the model was stable with power off but was unstable with power on and that the instability increased with increasing power. This result is very similar to that reported for another jet-flap model which had the engines located relatively far inboard (see ref. 4). In reference 4 it was found from smoke-flow studies that the tail was immersed in a downwash field that was particularly powerful because of the high concentration of lift on the inboard sections of the wing. This inboard concentration of lift caused a large and powerful tip vortex to be located far inboard in the region of the horizontal tail. Smoke-flow studies in the present investigation showed flow patterns in the vicinity of the tail similar to those reported in reference 4. It was therefore decided to raise the horizontal tail and move it forward in an attempt to place it in a better flow field.

The results of tests with the tail in the high forward position (see fig. 9(a)) show that longitudinal stability was achieved even at the higher power settings. A pitch-up was introduced with this high tail location but the pitch-up did not occur until after the stall. In figure 9(c) the unstable slopes in the pitching-moment curves at low angles of attack for the power-on conditions are a result of tail stall. Such a result points out the need for effective high-lift devices on the tail to provide adequate trim and control for a configuration of this type. It should be noted that the tail is not as effective on the model as it would be on an airplane, even though it is equipped with high-lift devices, because of the low scale of the tests. Since the high forward tail position provided generally satisfactory stability and trim characteristics, all subsequent tests were made with this tail position. The stability and trim characteristics for a trailing-edge flap deflection of $30^{\circ}/60^{\circ}$ (fig. 10) are not significantly different from those for a flap deflection of $20^{\circ}/40^{\circ}$ (fig. 9).

The results of tests to determine the lift characteristics of the horizontal tail (fig. 11) show that the basic tail had a maximum lift coefficient of only about 0.75. The addition of a leading-edge flap increased the maximum lift coefficient of the tail to about 1.4. A lift curve based on two-dimensional data corrected for aspect ratio, sweep, and taper ratio has been constructed for a clean horizontal tail, similar to that of the model,

for an assumed full-scale Reynolds number of 6×10^6 (based on the mean aerodynamic chord of the tail). This curve is presented in figure 11, and shows that the maximum lift coefficient of the tail with the leading-edge flap in these low-scale tests would be approximately the same as that obtained without leading-edge flaps at full scale. The addition of a leading-edge flap and an elevator increased the maximum lift coefficient of the tail to about 1.75. One significant point noted at negative angles of attack is that the leading-edge flap caused the lift-curve slope of the tail to decrease sharply, indicating flow separation on the bottom surface of the tail. Flow separation could alter appreciably the stability of an aircraft and is apparently caused by the relatively sharp nose of the flap. The use of a larger nose radius on the leading-edge flap would probably minimize or eliminate the problem.

The results of flow surveys to measure the downwash characteristics in the vicinity of the horizontal tail (figs. 12 to 14) indicate that the variation of downwash angle with tail spanwise station is not very large except for horizontal-tail positions near the fuselage ($z/\bar{c}$ near 0). For these positions, the downwash angle increases rapidly from the root to the tip station. A summary of the downwash measurements in terms of the downwash factor $1 - \frac{\partial \epsilon}{\partial \alpha}$ (presented in fig. 15) shows that for the horizontal tail to retain even minimal effectiveness at the high thrust coefficients used in jet-flap operation, it must be located at least 1.5 or 2 chords above the fuselage.

Lateral Stability With Symmetric Thrust

The static lateral stability characteristics of the configuration under conditions of symmetric thrust are presented in figures 16 to 18 for various flap deflections and thrust levels. These figures include some tail-off data, and all tail-on data are for the configuration with high forward tail. Figure 16 shows that the lateral characteristics are very nearly linear functions of sideslip angle between -5° and 5°.

Figures 17 and 18 show the variation with angle of attack of the static lateral stability derivatives as determined from tests at sideslip angles of 5° and -5°. These data show that the tail-on configuration had positive directional stability $\left(C_{n_\beta}\right)$ and positive effective dihedral $\left(-C_{l_\beta}\right)$ at any test condition below the stall. In general the directional stability and effective dihedral are not affected greatly by changes in trailing-edge flap deflection at angles of attack below 10°. The directional stability is, however, markedly increased by the application of thrust at flap deflections of $20^\circ/40^\circ$ and $30^\circ/60^\circ$. A comparison of the tail-on data of figure 17 with the tail-off data of figure 18 shows that the vertical tail remained effective for directional stability up through the stall. The loss in directional stability above the stall, as indicated by the data of figure 17, is a result of the large increase in instability of the wing-fuselage combination. Note that the application of power caused the tail-off configuration with $30^\circ/60^\circ$ flap deflection to become directionally stable over most of the unstalled range.

Lateral and Longitudinal Characteristics With Asymmetric Thrust

Asymmetric thrust (one engine inoperative) would be expected to produce lateral trim problems for any configuration. Because in a powered-lift system engine failure also results in loss of lift, plots of the lateral characteristics with one engine out are accompanied by the corresponding longitudinal data. These data are presented in figures 19 to 22.

With one engine inoperative, probably the most noteworthy lateral trim characteristic is the large rolling moment. Figures 20(a) and 20(b), for example, show that for high thrust and large flap deflection $\left(C_\mu = 2.90;\ \delta_{f1}/\delta_{f2} = 30^o/60^o\right)$, out-of-trim rolling-moment coefficients of about 0.20 would accompany the failure of one outboard engine even at angles of attack well below the stall. At or near the stall the moments become much larger because stall occurs at a lower angle of attack behind an inoperative engine. The corresponding lift data (fig. 20(c)), when corrected to pitch trim and compared with the four-engine data of figure 5(b), show that the engine failure would produce a loss in lift coefficient of about 1.0. Further lift losses would probably be introduced in trimming the lateral moments.

Loss of one outboard engine can also produce large yawing moments. Data from figures 19(a) and 19(b) show out-of-trim yawing-moment coefficients of about 0.10 under high-thrust conditions through the usable range of angle of attack. As was the case in roll, the out-of-trim moment increases sharply as the stall is approached.

Lateral and longitudinal data are also presented (figs. 21 and 22) for the case of one inboard engine inoperative. The lateral plots show out-of-trim moments which are still large, but they are appreciably smaller than those for the case of an outboard-engine inoperative. The lift data for the condition of one inboard engine inoperative appear to be essentially the same as for the case of one outboard engine inoperative.

Lateral and Longitudinal Characteristics With Asymmetric Control Deflection

The lateral control moments which were produced by a conventional rudder, conventional ailerons, and two spoiler systems are shown in figures 23 to 26. Longitudinal data for the spoiler systems are presented in figures 27 and 28.

The increments in lateral coefficients produced by 15^o of rudder deflection are presented in figure 23 for various flap deflections and thrust levels. Yawing-moment coefficients are approximately 0.02, and are virtually unaffected by changes in thrust, angle of attack, or flap deflection. A comparison of these control moments with the previously-discussed out-of-trim moments resulting from engine-out operation (figs. 19 to 22) indicate that under many operating conditions a conventional rudder could not restore directional trim in event of an engine failure.

The lateral effects produced by aileron deflection with all four engines operating (right aileron -25°, left aileron $+15^{\circ}$) are presented in figure 24. The maximum incremental rolling-moment coefficient attained in the operational angle-of-attack range was 0.06, approximately one-quarter of what would be required for trim in an engine-out condition.

Figure 25 shows that conventional spoilers (located on the wing just forward of the flap system) are not capable of producing rolling moments large enough to provide engine-out trim. The conventional spoilers in combination with a small-chord spoiler on the flap itself, however, produced rolling moments about equal to those required for engine-out trim. (See fig. 26.) Of course, the use of spoilers for roll trim in the engine-out condition severely reduces the total lift capability of a configuration. Longitudinal data for spoiler operation (figs. 27 and 28) show that under the conditions in which the rolling moments required for trim are produced, there are decrements of approximately 1.0 in lift coefficient. In an engine-out situation, this lift loss due to spoiler operation would be on the wing on which two engines were still operating, and consequently would be in addition to the lift loss on the other wing caused directly by the failure of the engine.

The use of differential trailing-edge flap deflection to restore roll trim in an engine-out condition produces the lateral and longitudinal effects presented in figures 29(a) and 29(b). Although sizable rolling moments are produced by differential deflection, they are considerably less than required to trim the moments produced by engine failure in the $30^{\circ}/60^{\circ}$ flap configuration, and are accompanied by large adverse yawing moments. Lift coefficients for the differentially deflected flap configuration are about the same as those for the symmetric $20^{\circ}/40^{\circ}$ flap system.

SUMMARY OF RESULTS

From a wind-tunnel investigation of a jet transport configuration that has a high thrust-weight ratio and is equipped with an external-flow jet flap, the following results were obtained:

1. Maximum lift coefficients of abcut 8 were measured for test conditions which simulated a jet transport configuration having a thrust-weight ratio of about 0.5.

2. Longitudinal instability was encountered at high thrust coefficients because of adverse downwash variations in the vicinity of the tail. This problem was solved by raising the tail and moving it forward to a more favorable downwash field.

3. The model was laterally and directionally stable under all power conditions. Increases in thrust produced increases in directional stability and dihedral effect.

4. In the powered lift conditions, loss of thrust of an engine produced rolling and yawing moments which could not be trimmed out through conventional aileron and rudder controls; the use of spoilers alone provided enough roll control to trim out these rolling moments but the lift loss associated with the use of spoilers was severe.

Langley Research Center,
National Aeronautics and Space Administration,
Hampton, Va., July 23, 1970.

REFERENCES

1. Campbell, John P.; and Johnson, Joseph L., Jr.: Wind-Tunnel Investigation of an External-Flow Jet-Augmented Slotted Flap Suitable for Application to Airplanes With Pod-Mounted Jet Engines. NACA TN 3898, 1956.

2. Johnson, Joseph L., Jr.: Wind-Tunnel Investigation of the Static Longitudinal Stability and Trim Characteristics of a Sweptback-Wing Jet-Transport Model Equipped With an External-Flow Jet-Augmented Flap. NACA TN 4177, 1958.

3. Johnson, Joseph L., Jr.: Wind-Tunnel Investigation of a Small-Scale Sweptback-Wing Jet-Transport Model Equipped With an External-Flow Jet-Augmented Double Slotted Flap. NASA MEMO 3-8-59L, 1959.

4. Parlett, Lysle P.; and Shivers, James P.: Wind-Tunnel Investigation of an STOL Aircraft Configuration Equipped With an External-Flow Jet Flap. NASA TN D-5364, 1969.

5. Freeman, Delma C., Jr.; Grafton, Sue B.; and D'Amato, Richard: Static and Dynamic Stability Derivatives of a Model of a Jet Transport Equipped With External-Flow Jet-Augmented Flaps. NASA TN D-5408, 1969.

6. Mechtly, E. A.: The International System of Units – Physical Constants and Conversion Factors. NASA SP-7012, 1964.

TABLE I.- DIMENSIONS OF MODEL

Wing:		
Area, ft^2 (m^2)	7.87	(0.731)
Span, in. (cm)	95.08	(241.51)
Aspect ratio	7.75	
Length of mean aerodynamic chord, in. (cm)	13.22	(33.59)
Distance from nose of model to quarter-chord point of mean aerodynamic chord, in. (cm)	40.54	(102.98)
Spanwise station of mean aerodynamic chord, in. (cm)	19.33	(49.10)
Root chord, in. (cm)	19.49	(49.50)
Tip chord (theoretical tip), in. (cm)	6.54	(16.62)
Break-station chord, in. (cm)	12.08	(30.67)
Spanwise station of break, in. (cm)	20.16	(51.20)
Sweep of quarter-chord line:		
Inboard panel, deg	24.08	
Outboard panel, deg	25.00	
Dihedral of quarter-chord line:		
Inboard panel, deg	-3.50	
Outboard panel, deg	-3.50	
Incidence of mean aerodynamic chord, deg	4.50	
Incidence of root chord, deg	6.00	
Geometric twist:		
Root, deg	0.0	
Break station, deg	-1.5	
Tip, deg	-3.5	
Aileron:		
Span, in. (cm)	9.38	(23.85)
Chord, outboard end, in. (cm)	2.34	(5.95)
Chord, inboard end, in. (cm)	2.97	(7.55)
Spanwise station of inboard end, in. (cm)	34.90	(88.70)
Hinge-line location, percent chord	70	
Sweep of hinge line, deg	20.2	
Vertical tail:		
Area, ft^2 (m^2)	1.77	(0.164)
Span, in. (cm)	19.47	(49.45)
Aspect ratio	1.69	

TABLE I.- DIMENSIONS OF MODEL – Concluded

Sweep angle:		
Leading edge, deg	37	
Trailing edge, deg	29.4	
Root chord, in. (cm)	13.94	(35.41)
Tip chord, in. (cm)	10.58	(26.87)
Rudder:		
Span, in. (cm)	16.53	(41.99)
Chord, upper end, parallel to X-axis, in. (cm)	2.67	(6.78)
Chord, lower end, perpendicular to hinge line, in. (cm)	2.72	(6.91)
Hinge-line location, percent vertical-tail chord	75	
Sweep of hinge line, deg	31.4	
Horizontal tail:		
Area, ft^2 (m^2)	2.88	(0.268)
Span, in. (cm)	46.76	(118.77)
Length of mean aerodynamic chord, in. (cm)	9.52	(24.18)
Incidence	Variable	
Elevator:		
Span, in. (cm)	17.31	(43.99)
Chord, outboard, in. (cm)	1.66	(4.21)
Chord, inboard, in. (cm)	3.31	(8.40)
Hinge-line location, percent horizontal-tail chord	73	
Sweep of hinge line, deg	16.5	
Engines:		
Spanwise location of inboard engines, in. (cm)	10.47	(26.59)
Spanwise location of outboard engines, in. (cm)	19.99	(50.77)
Incidence of all engine center lines relative to X-axis, deg	-3.00	
Moment reference:		
Longitudinal location, distance from nose of model, in. (cm)	43.14	(109.58)
Vertical location, distance from top of fuselage at wing, in. (cm)	4.92	(12.49)

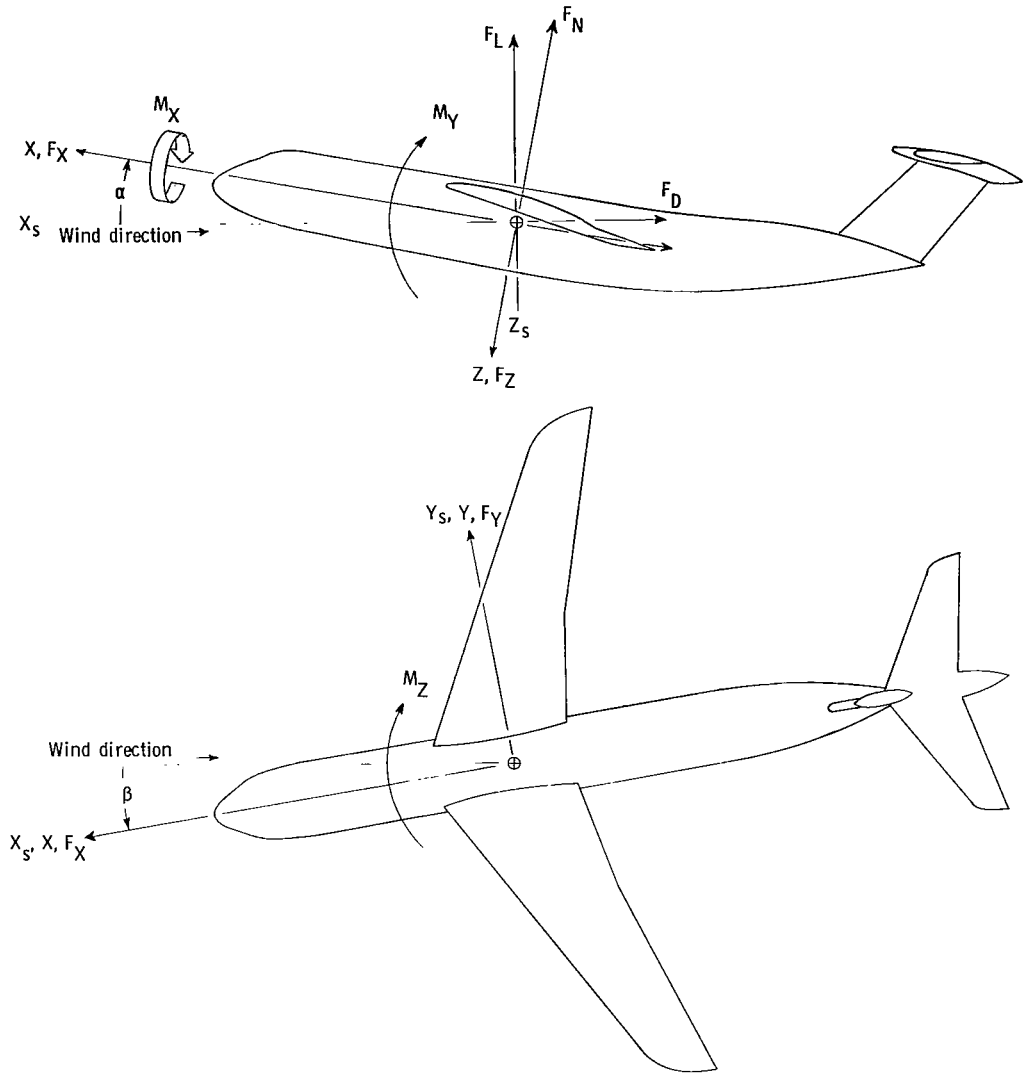

Figure 1.- Axis systems used in presentation of data. Arrows indicate positive direction of forces, moments, and angles.

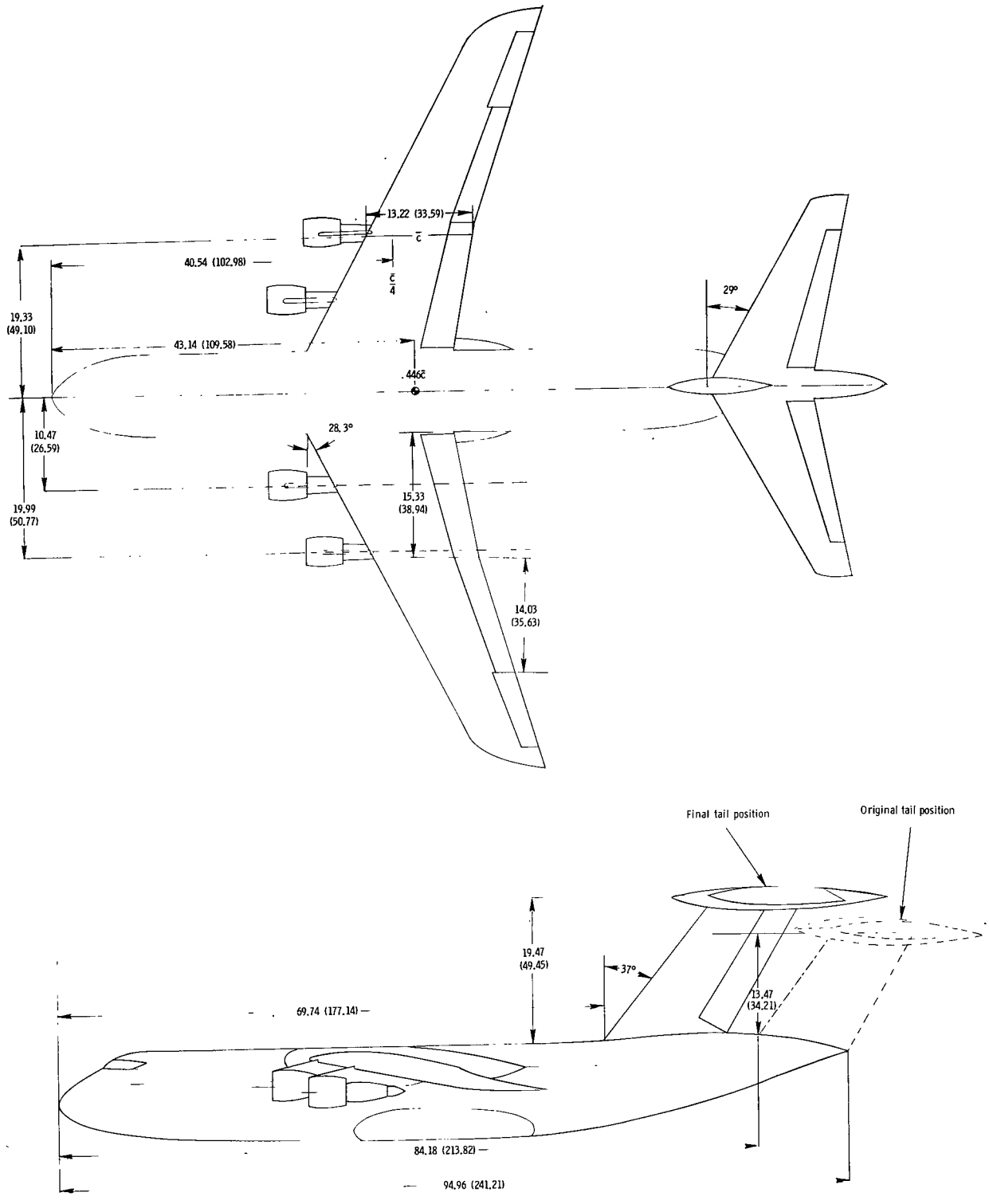

(a) Three-view drawing of complete model.

Figure 2.- Drawings of model used in investigation. All linear dimensions are in inches (centimeters).

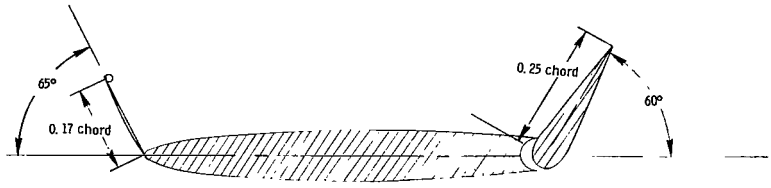

Cross section of horizontal tail

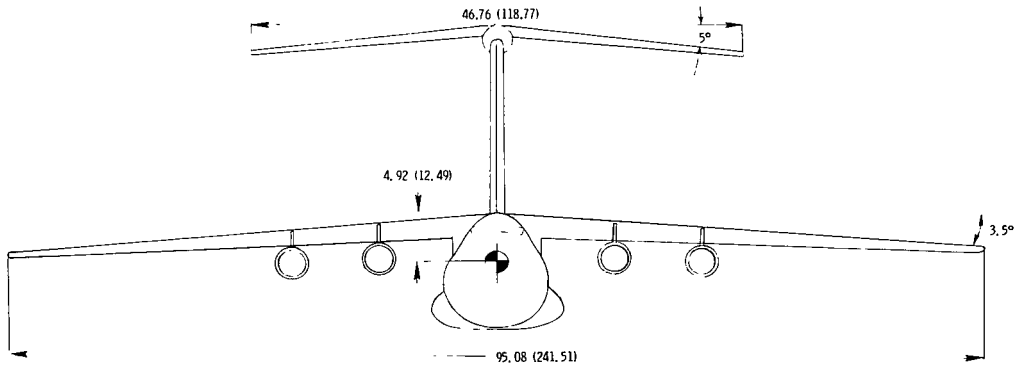

(a) Concluded.

Figure 2.- Continued.

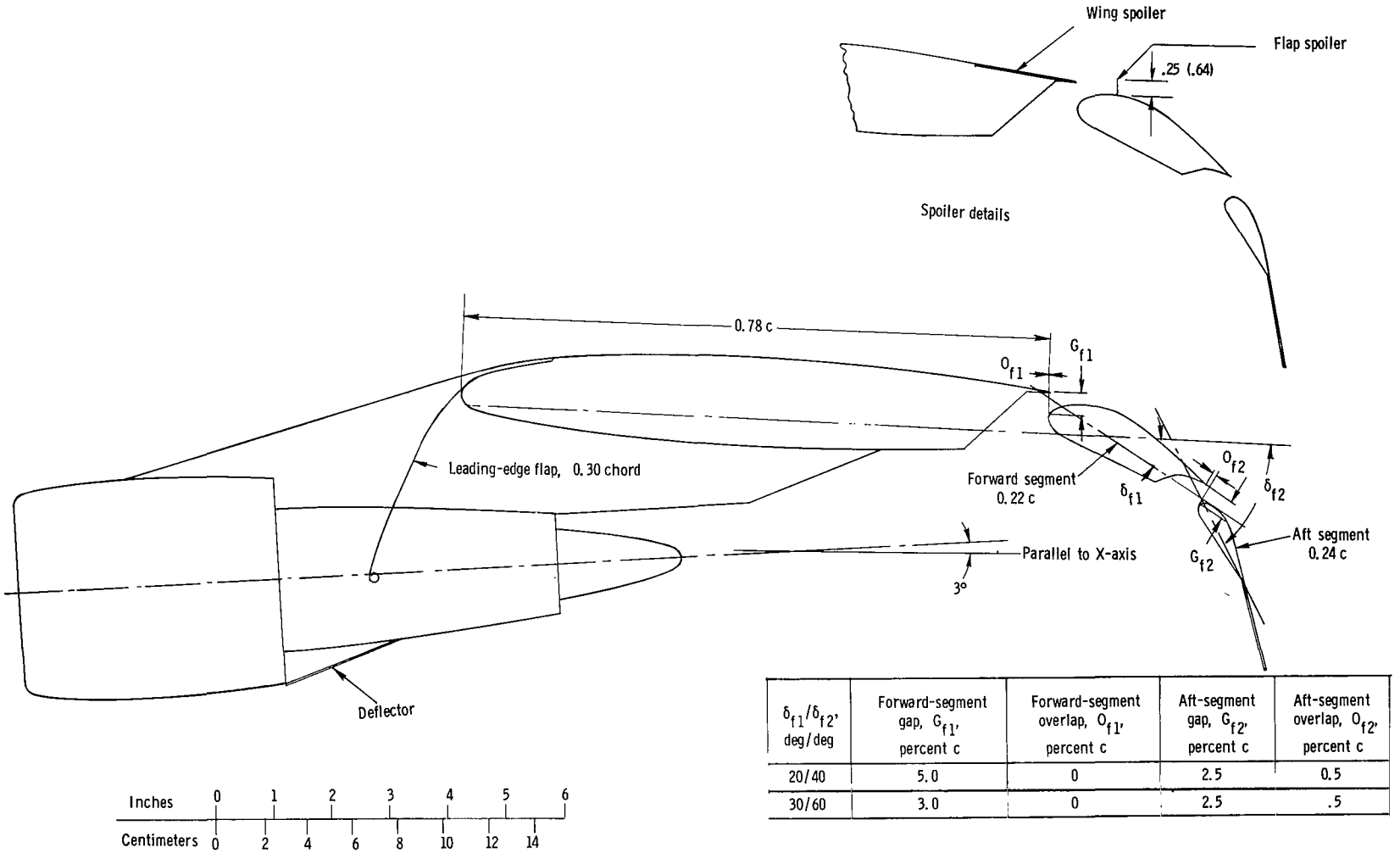

δ_{f1}/δ_{f2}, deg/deg	Forward-segment gap, G_{f1}, percent c	Forward-segment overlap, O_{f1}, percent c	Aft-segment gap, G_{f2}, percent c	Aft-segment overlap, O_{f2}, percent c
20/40	5.0	0	2.5	0.5
30/60	3.0	0	2.5	.5

(b) Flap assembly and engine-plyon details.

Figure 2.- Continued.

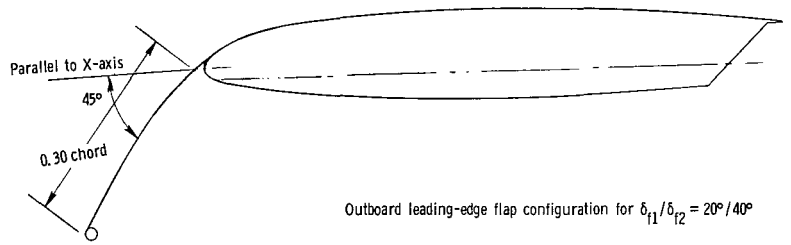

Outboard leading-edge flap configuration for $\delta_{f1}/\delta_{f2} = 20°/40°$

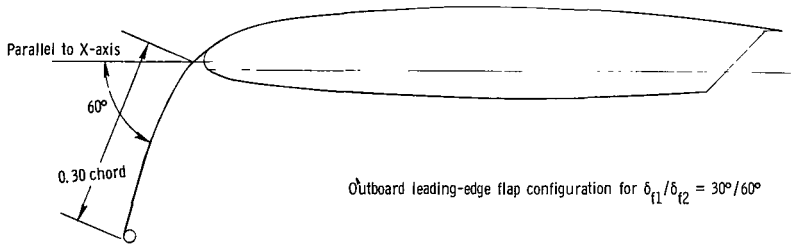

Outboard leading-edge flap configuration for $\delta_{f1}/\delta_{f2} = 30°/60°$

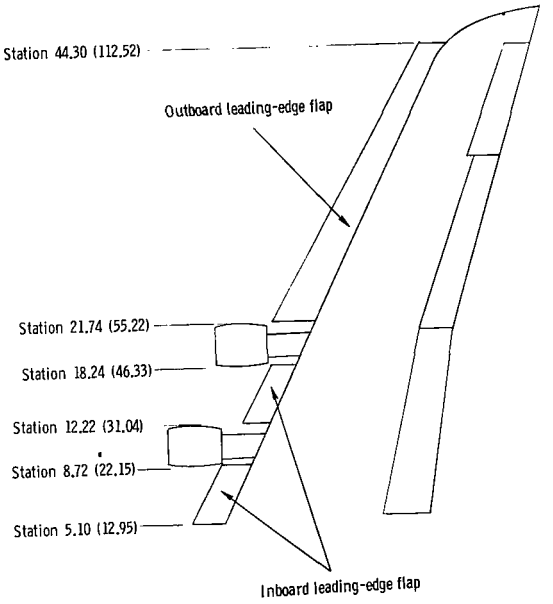

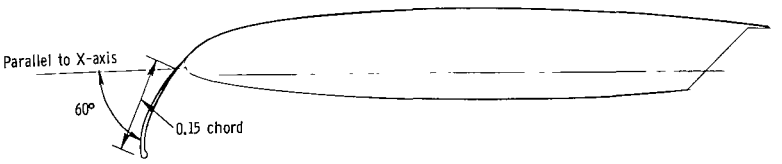

Inboard leading-edge flap configuration for both $\delta_{f1}/\delta_{f2} = 20°/40°$ and $\delta_{f1}/\delta_{f2} = 30°/60°$

(c) Leading-edge flap details. All dimensions are in inches (centimeters).

Figure 2.- Continued.

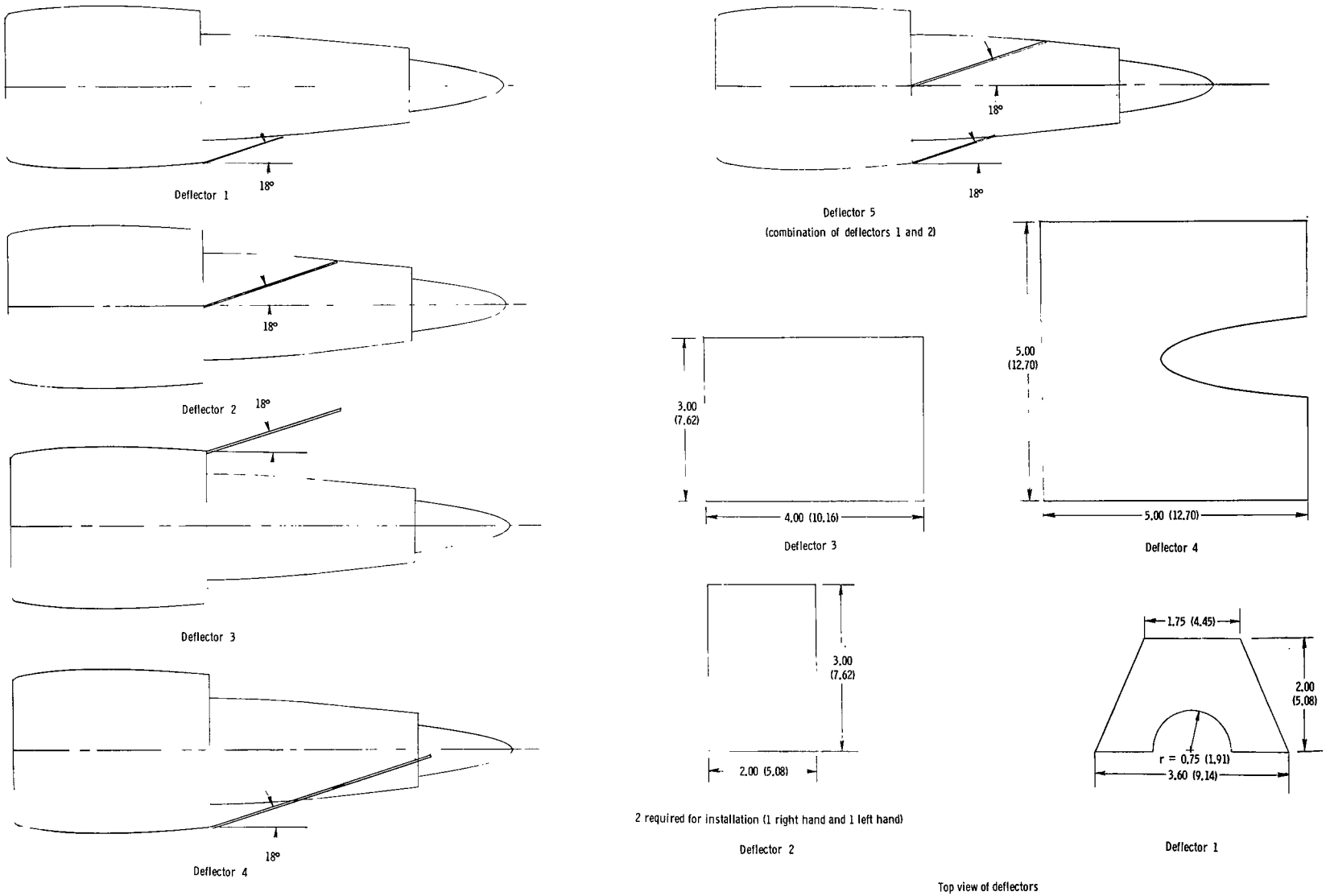

(d) Details of jet-exhaust deflectors. Dimensions are in inches (centimeters).

Figure 2.- Concluded.

L-69-4196

Figure 3.- Photograph of model used in investigation.

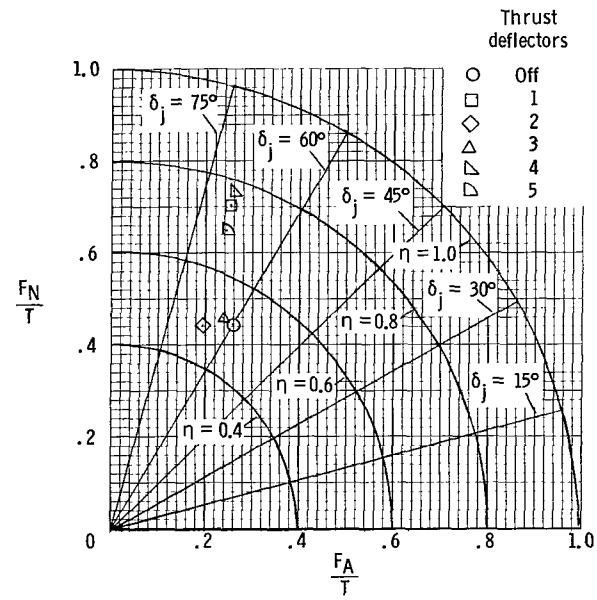

Figure 4.- Summary of turning efficiency and turning angle. $\delta_{f1}/\delta_{f2} = 30°/60°$.

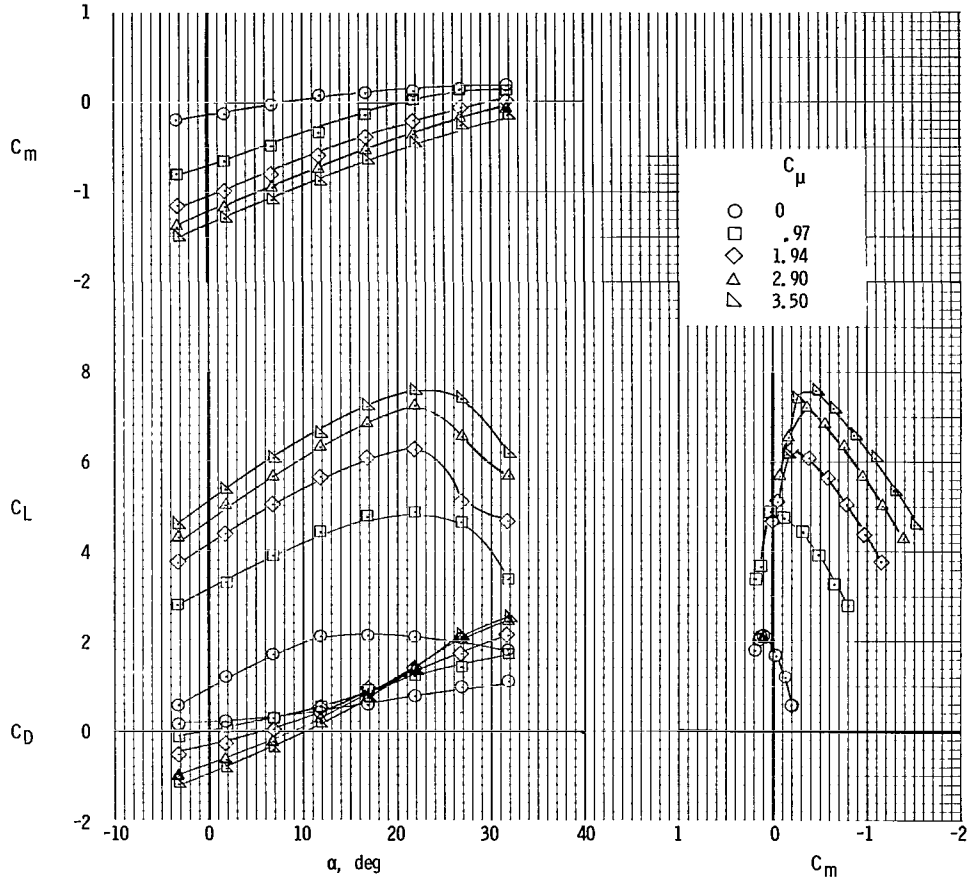

(a) $\delta_{f1}/\delta_{f2} = 20°/40°$.

Figure 5.- Longitudinal characteristics of the model with tail off.

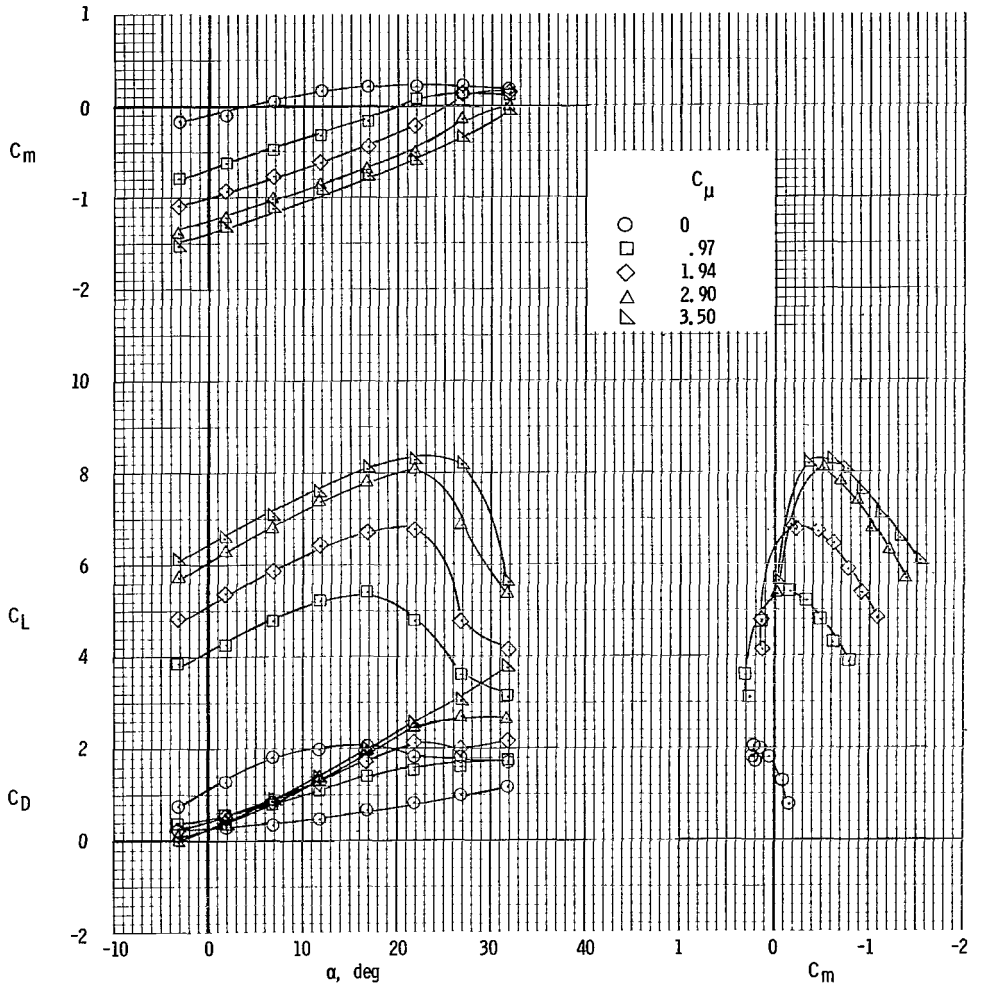

(b) $\delta_{f1}/\delta_{f2} = 30°/60°$.

Figure 5.- Concluded.

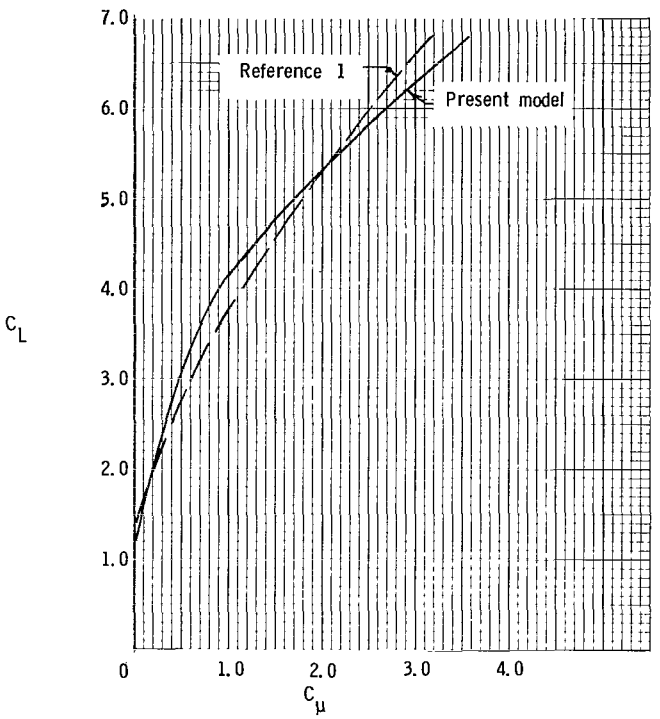

Figure 6.- Comparison of lift characteristics of two models with tail off. $\alpha = 0^\circ$; $\delta_{f1}/\delta_{f2} = 30^\circ/60^\circ$.

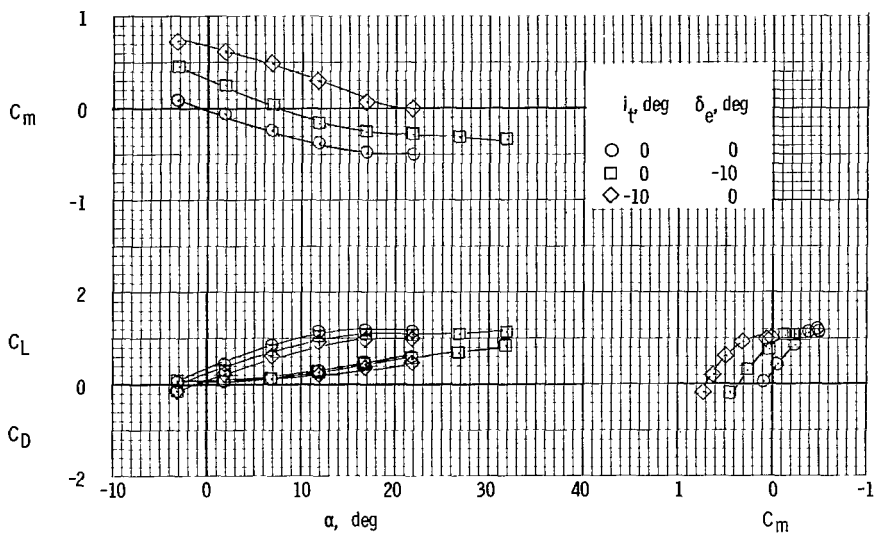

Figure 7.- Longitudinal characteristics of the model with tail on. $C_\mu = 0$.

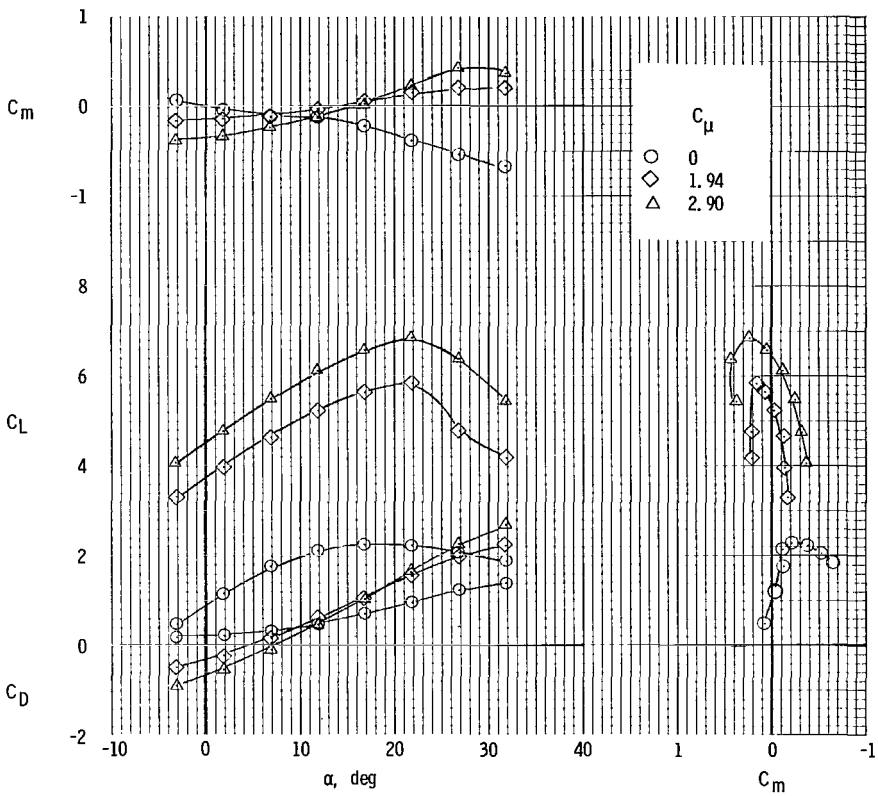

Figure 8.- Longitudinal characteristics of the model with horizontal tail in original position. $\delta_{f1}/\delta_{f2} = 20^\circ/40^\circ$; $i_t = 0^\circ$; $\delta_e = -50^\circ$.

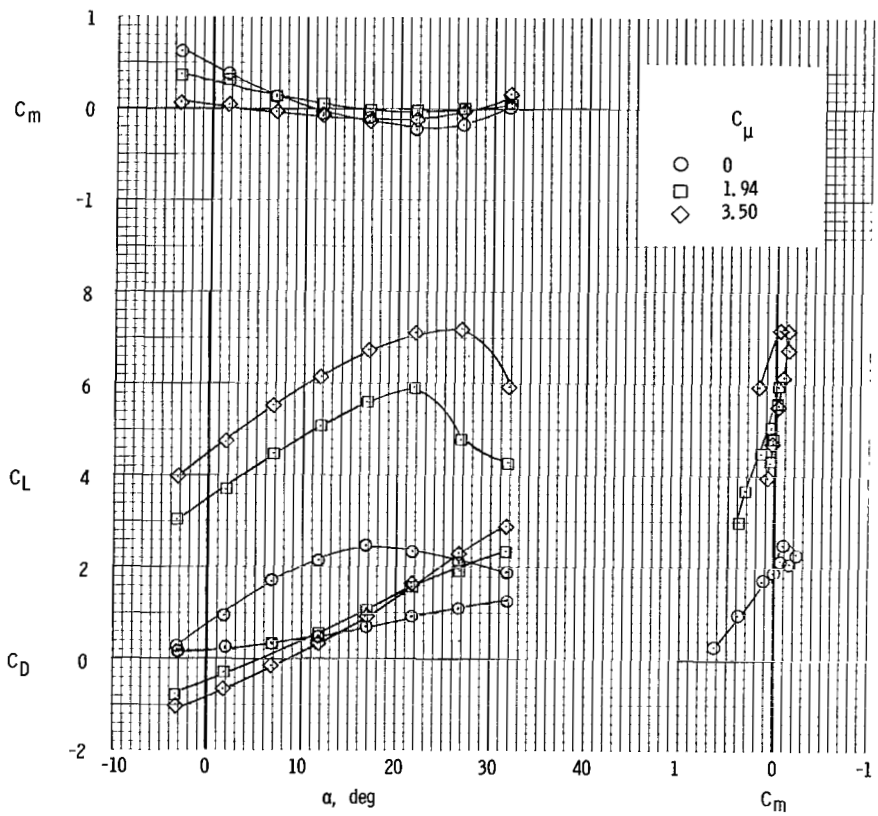

(a) $i_t = 0^\circ$.

Figure 9.- Longitudinal characteristics of the model with horizontal tail in high forward position and $\delta_{f1}/\delta_{f2} = 20^\circ/40^\circ$. $\delta_e = -50^\circ$.

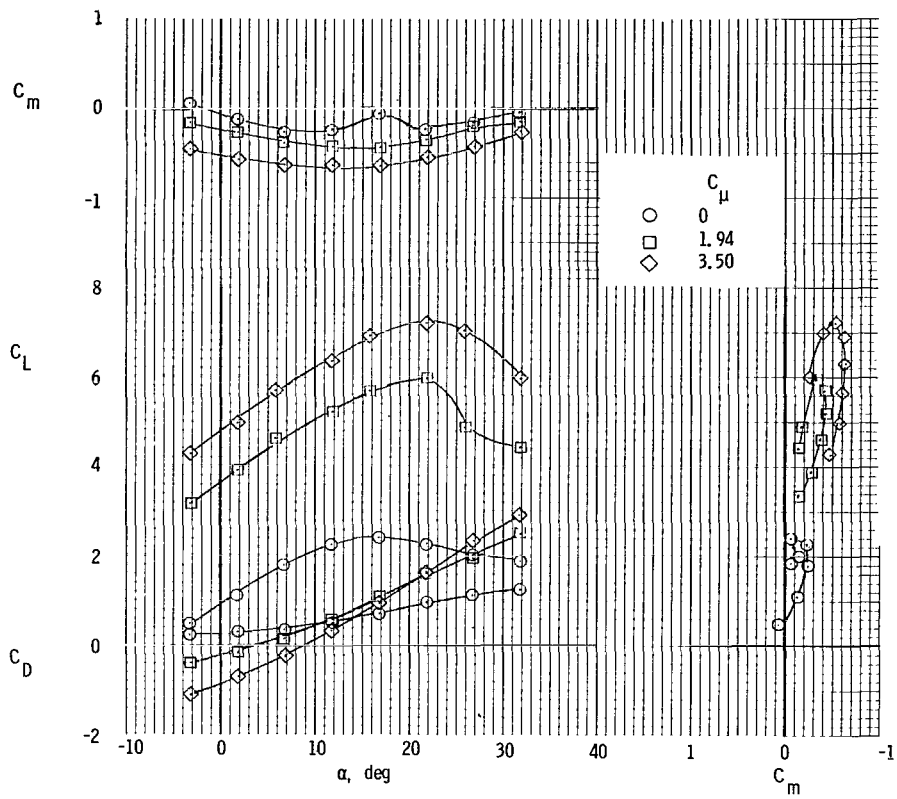

(b) $i_t = 5^\circ$.

Figure 9.- Continued.

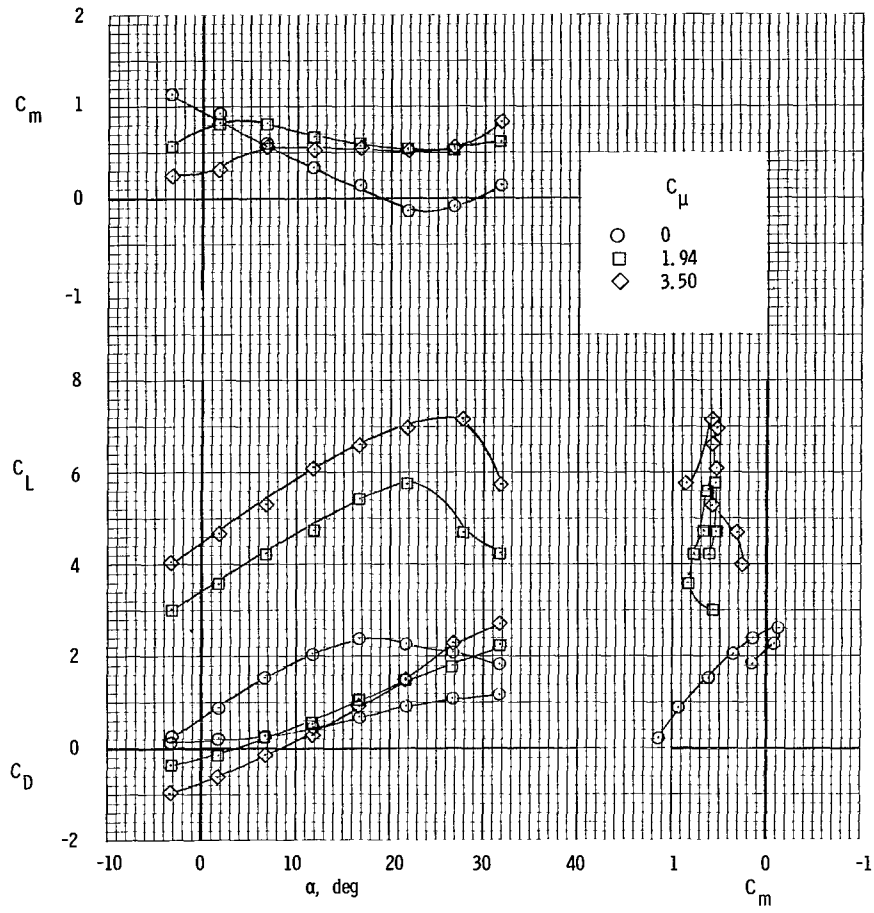

(c) $i_t = -5^\circ$.

Figure 9.- Concluded.

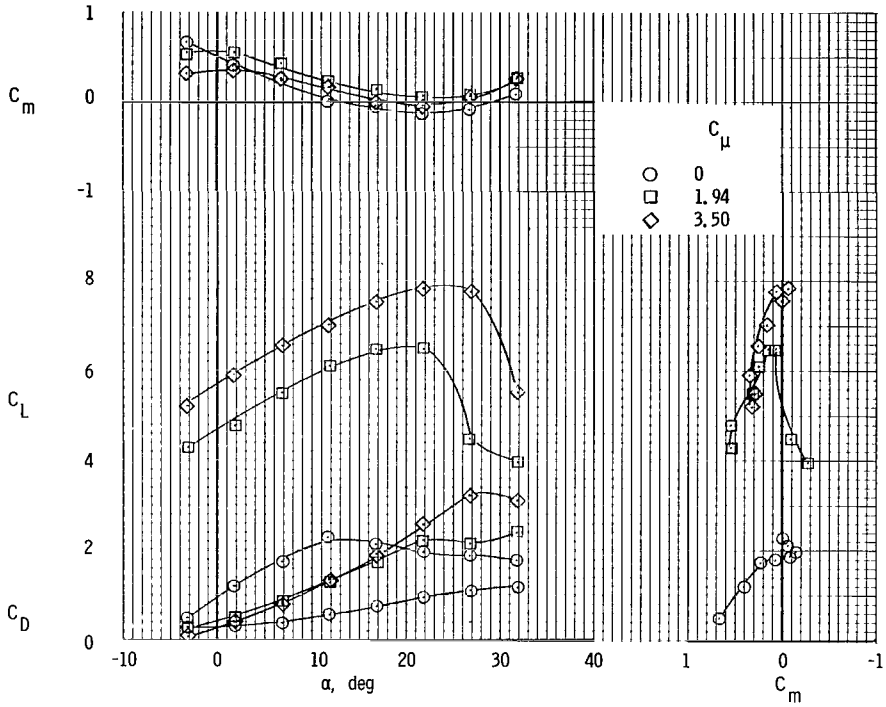

(a) $i_t = 0^\circ$.

Figure 10.- Longitudinal characteristics of the model with horizontal tail in high forward position and $\delta_{f1}/\delta_{f2} = 30^\circ/60^\circ$. $\delta_e = -50^\circ$.

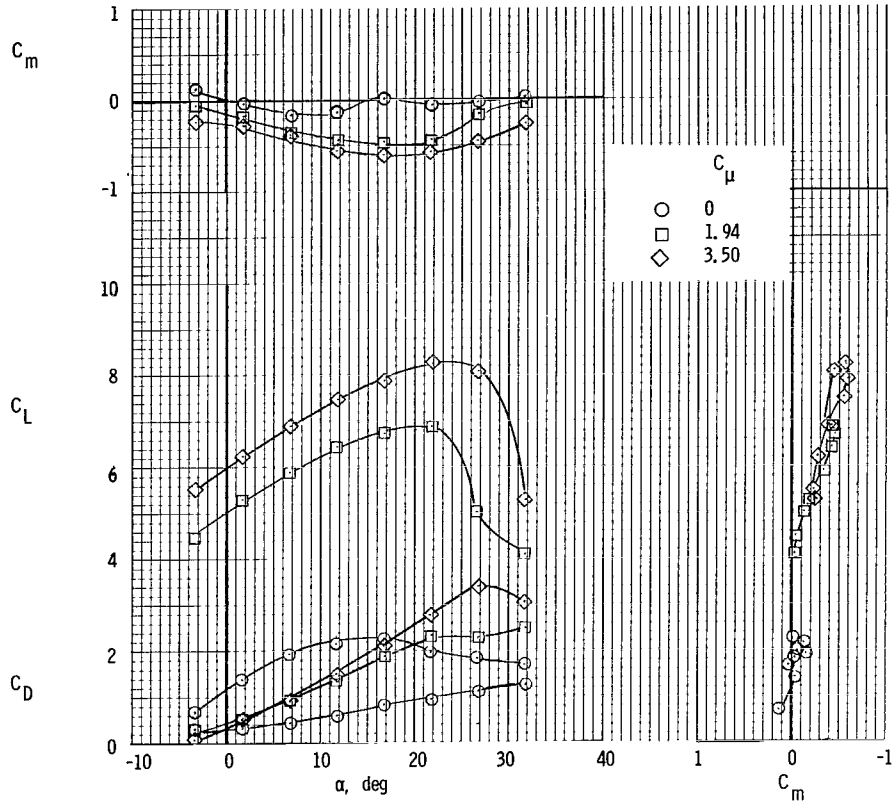

(b) $i_t = 5^\circ$.

Figure 10.- Continued.

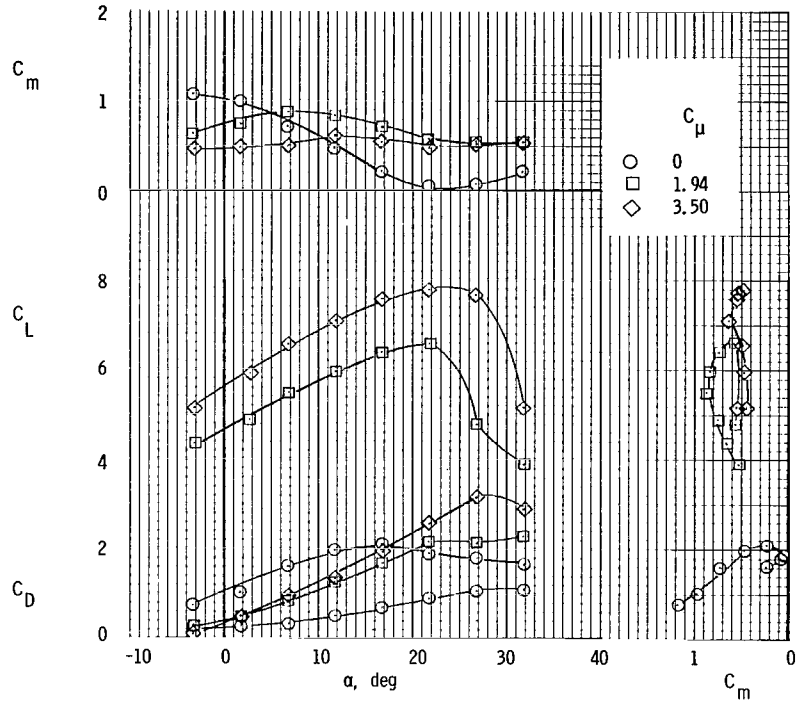

(c) $i_t = -5^\circ$.

Figure 10.- Concluded.

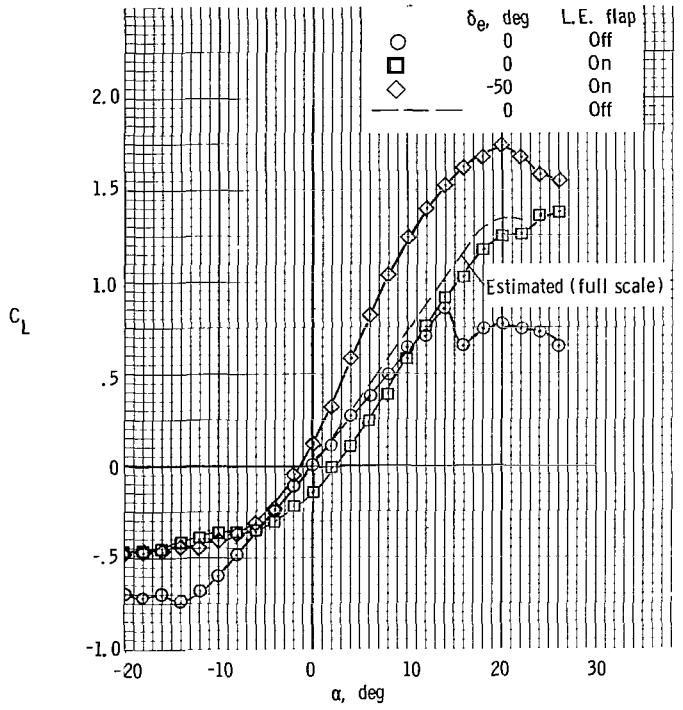

Figure 11.- Lift characteristics of horizontal tail.

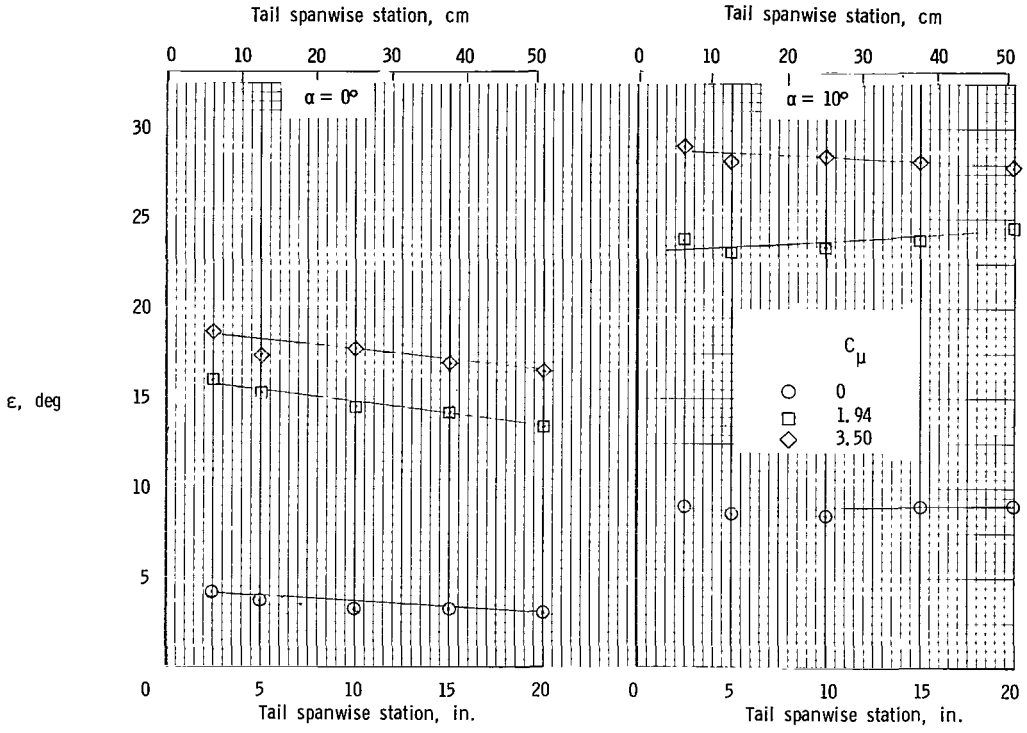

(a) $z/\bar{c} = 1.0$.

Figure 12.- Variation of downwash angle with tail spanwise station for $l/\bar{c} = 4.0$. $\delta_{f1}/\delta_{f2} = 30°/60°$.

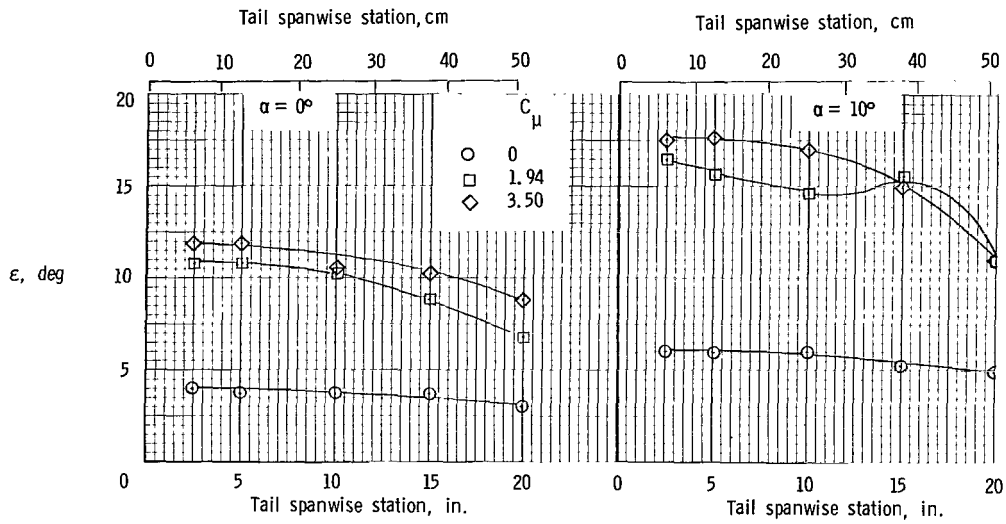

(b) $z/\bar{c} = 2.0$.

Figure 12.- Continued.

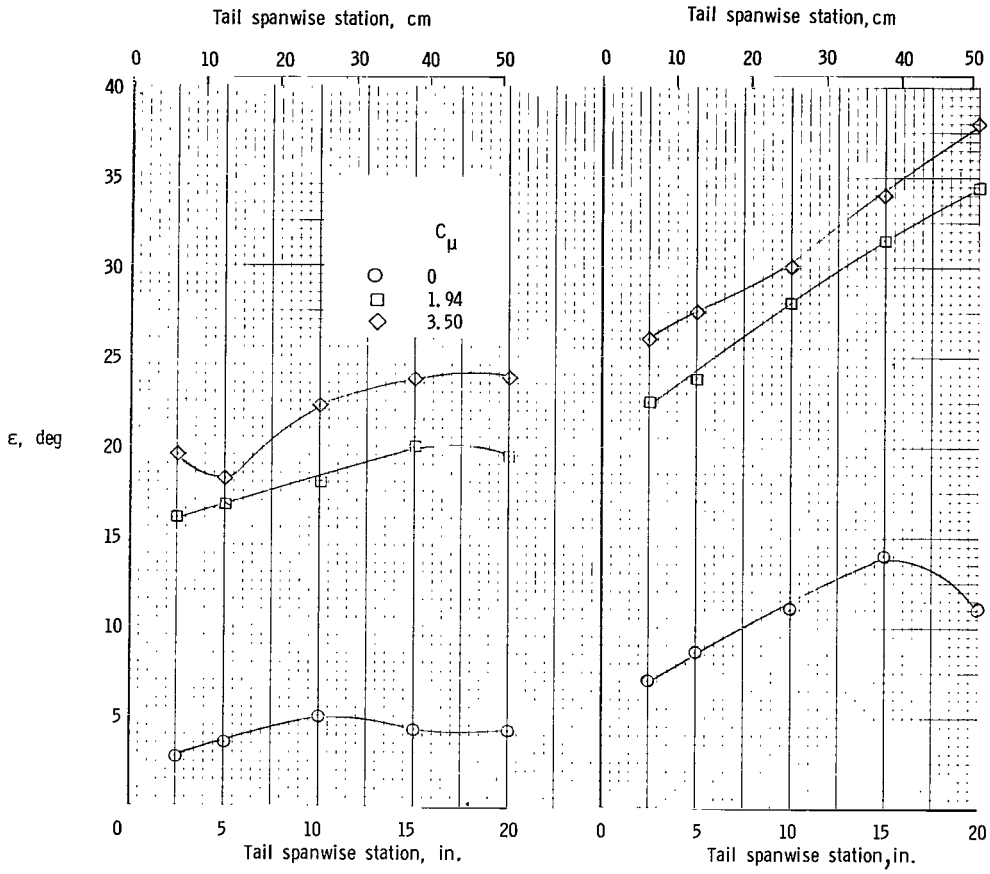

(c) $z/\bar{c} = 0.$

Figure 12.- Concluded.

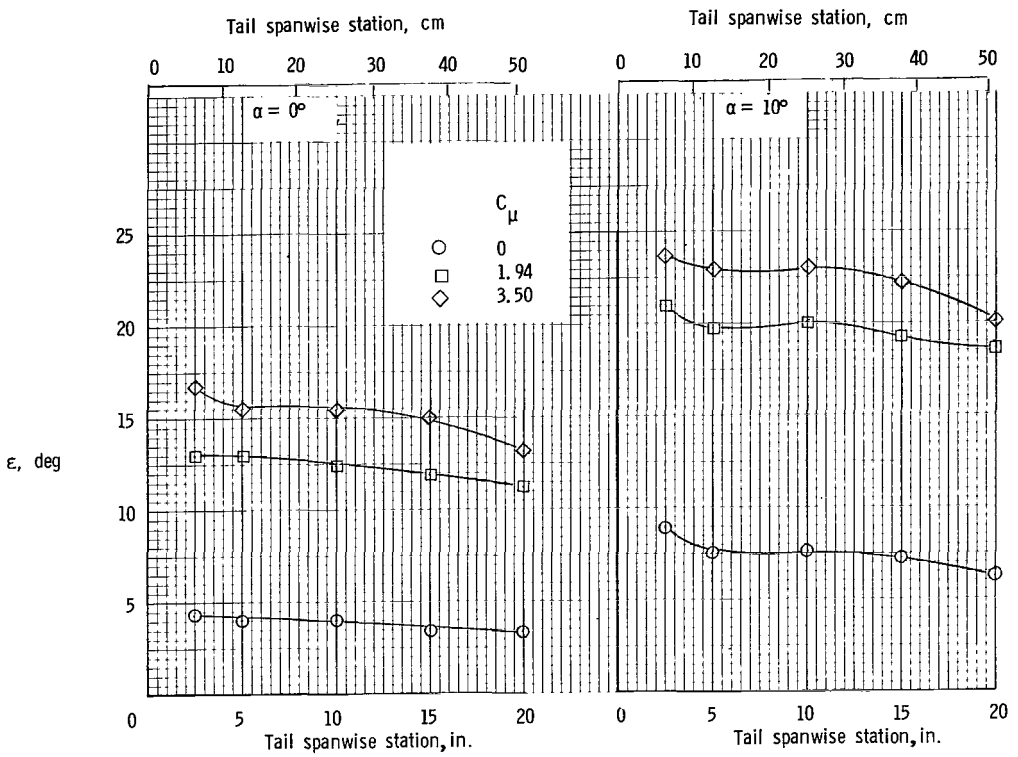

(a) $z/\bar{c} = 1.5$.

Figure 13.- Variation of downwash angle with tail spanwise station for $l/\bar{c} = 3.0$. $\delta_{f1}/\delta_{f2} = 30°/60°$.

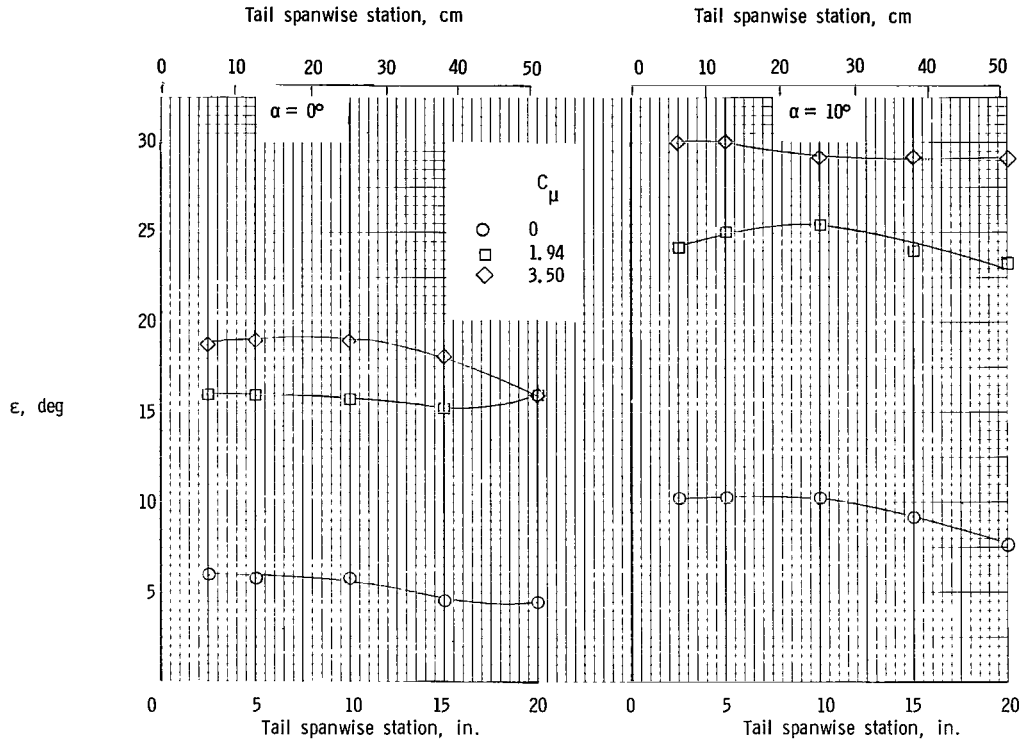

(b) $z/\bar{c} = 1.0$.

Figure 13.- Concluded.

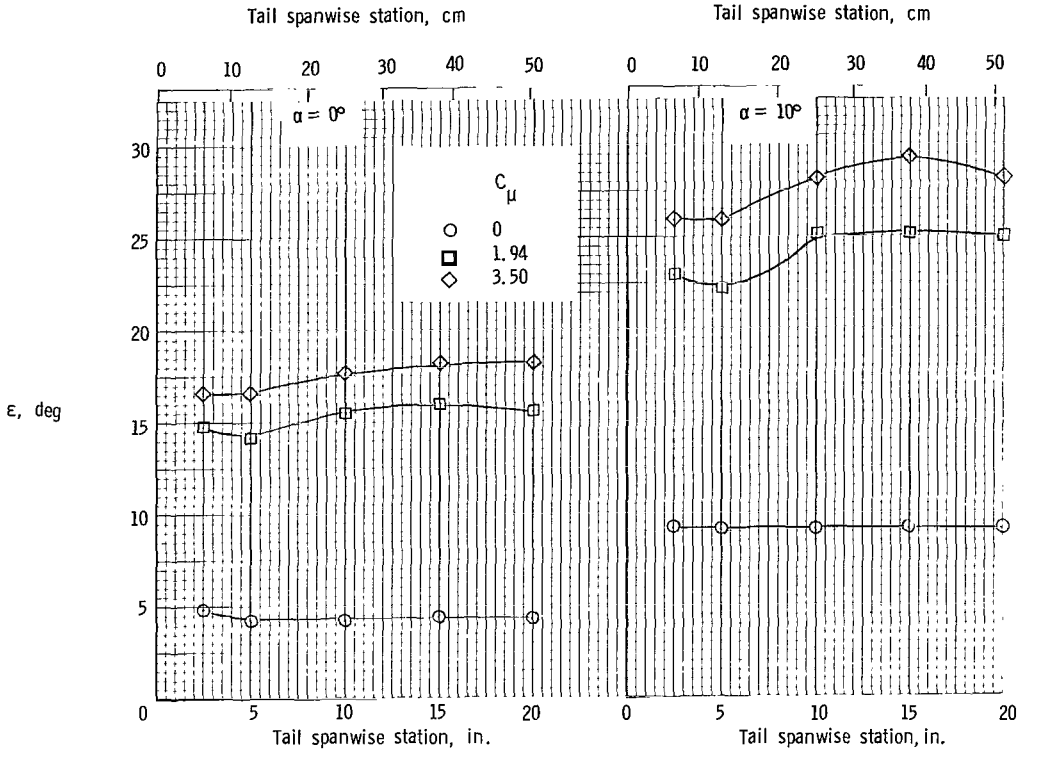

Figure 14.- Variation of downwash with tail spanwise station for $l/\bar{c} = 2.0$. $\delta_{f1}/\delta_{f2} = 30°/60°$; $z/\bar{c} = 1.0$.

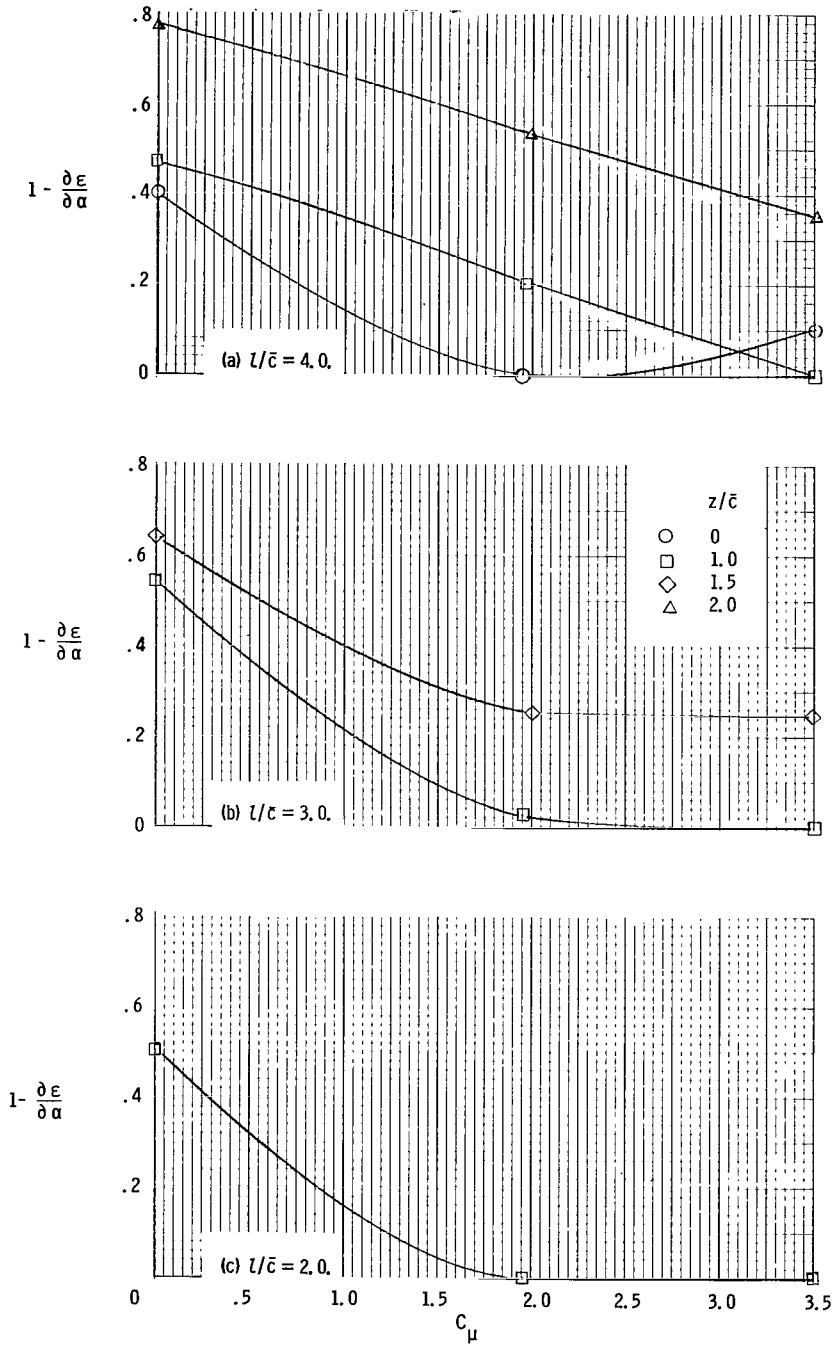

Figure 15.- Summary of downwash flow studies.
$\delta_{f1}/\delta_{f2} = 30^{o}/60^{o}$.

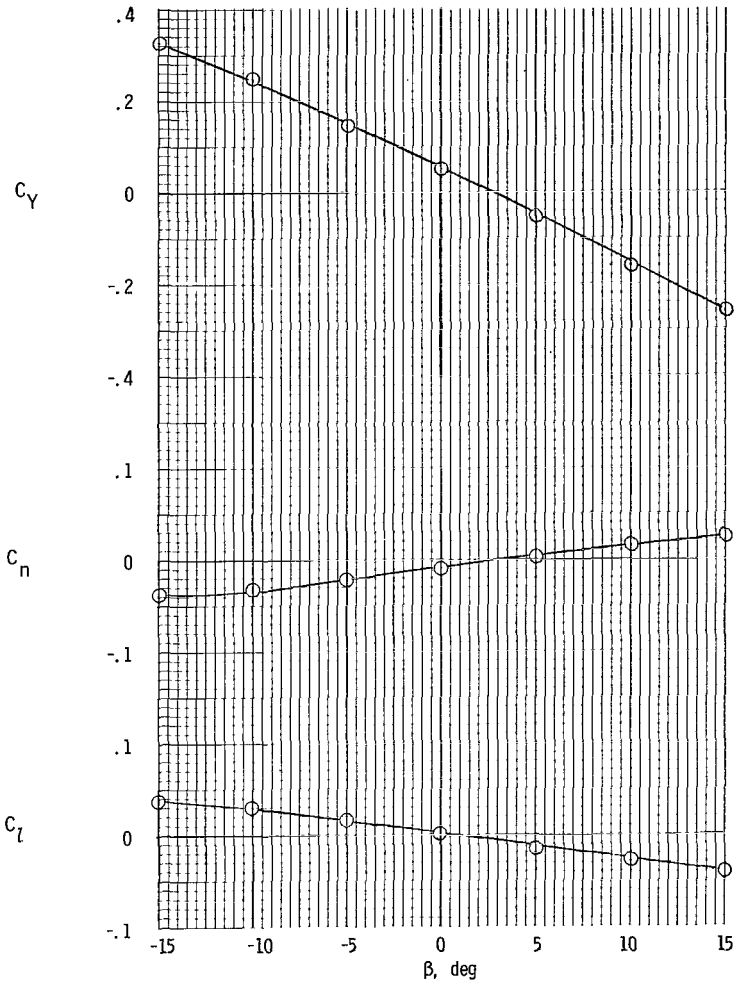

(a) $\delta_{f1}/\delta_{f2} = 0^\circ$; $\delta_e = 0^\circ$; $C_\mu = 0$.

Figure 16.- Variation of lateral characteristics with sideslip angle. $\alpha = 5^\circ$; $i_t = 0^\circ$.

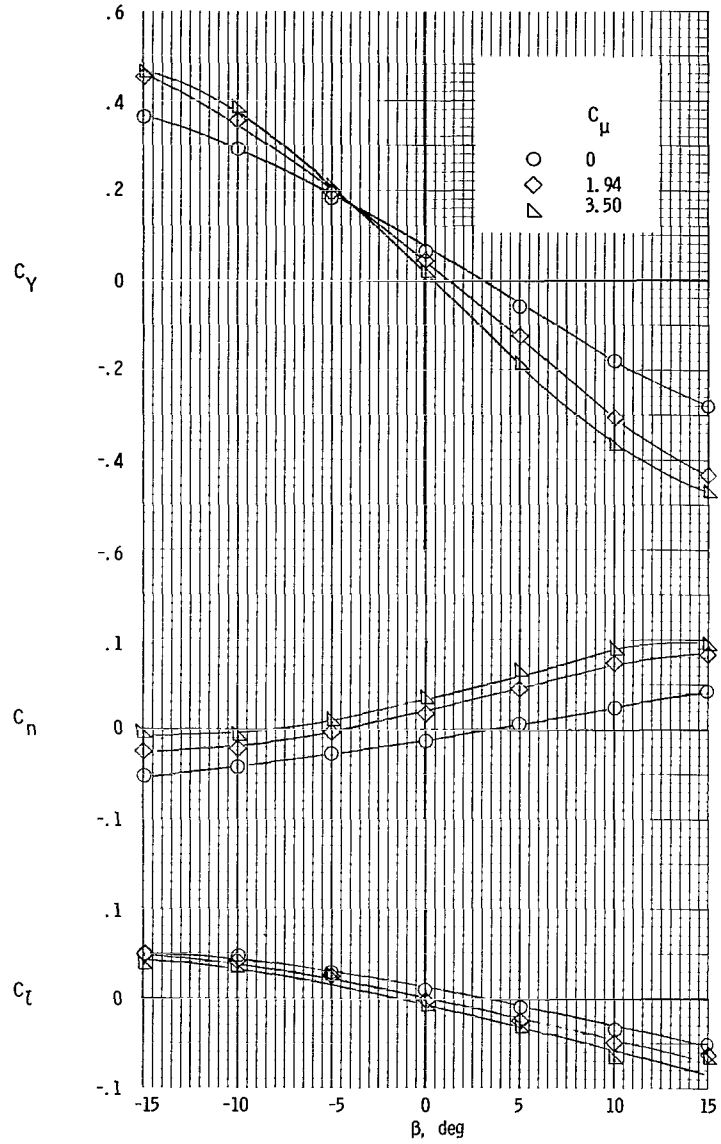

(b) $\delta_{f1}/\delta_{f2} = 20°/40°$; $\delta_e = -50°$.

Figure 16.- Continued.

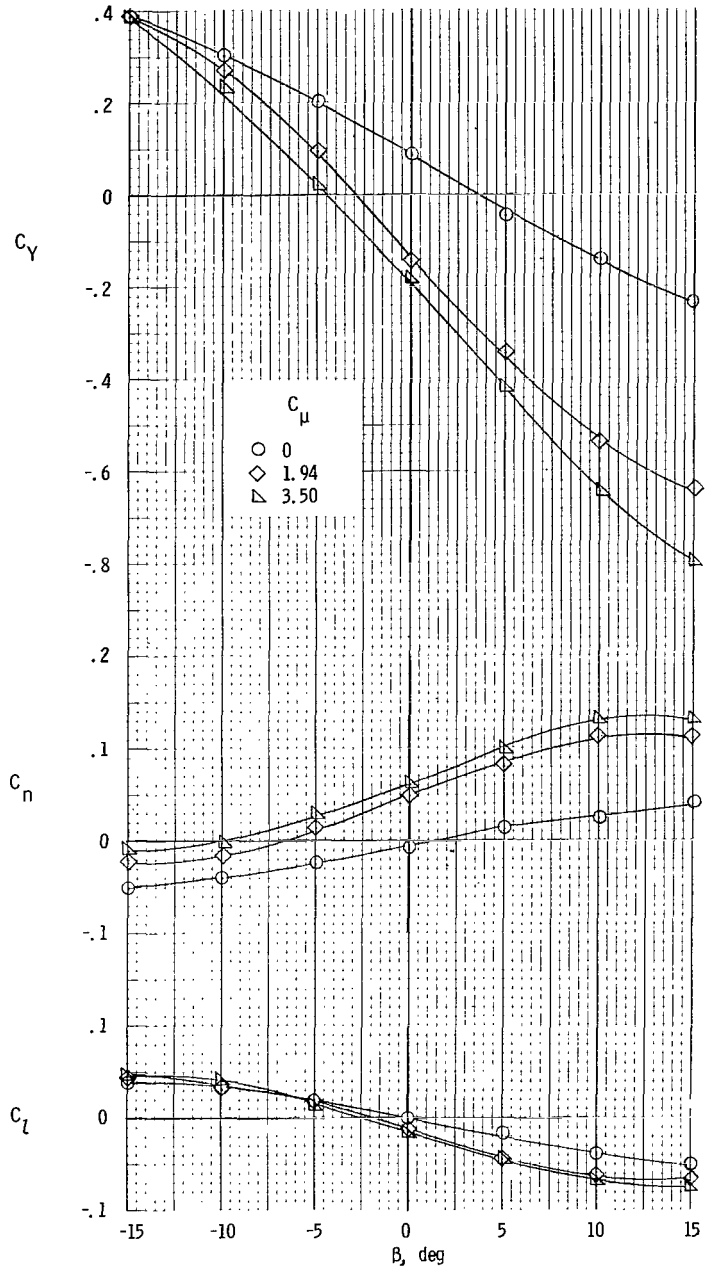

(c) $\delta_{f1}/\delta_{f2} = 30^\circ/60^\circ$; $\delta_e = -50^\circ$.

Figure 16.- Concluded.

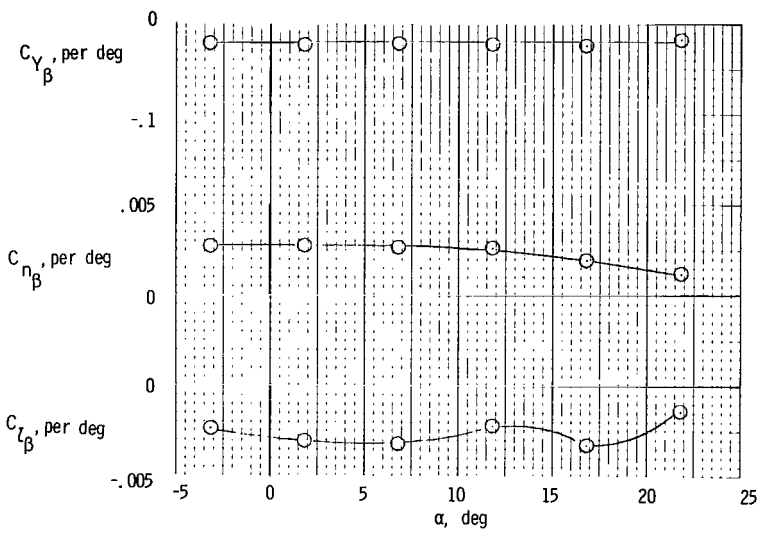

(a) $\delta_{f1}/\delta_{f2} = 0^{\circ}$; $C_\mu = 0$.

Figure 17.- Lateral stability characteristics of the model with horizontal tail in high forward position.

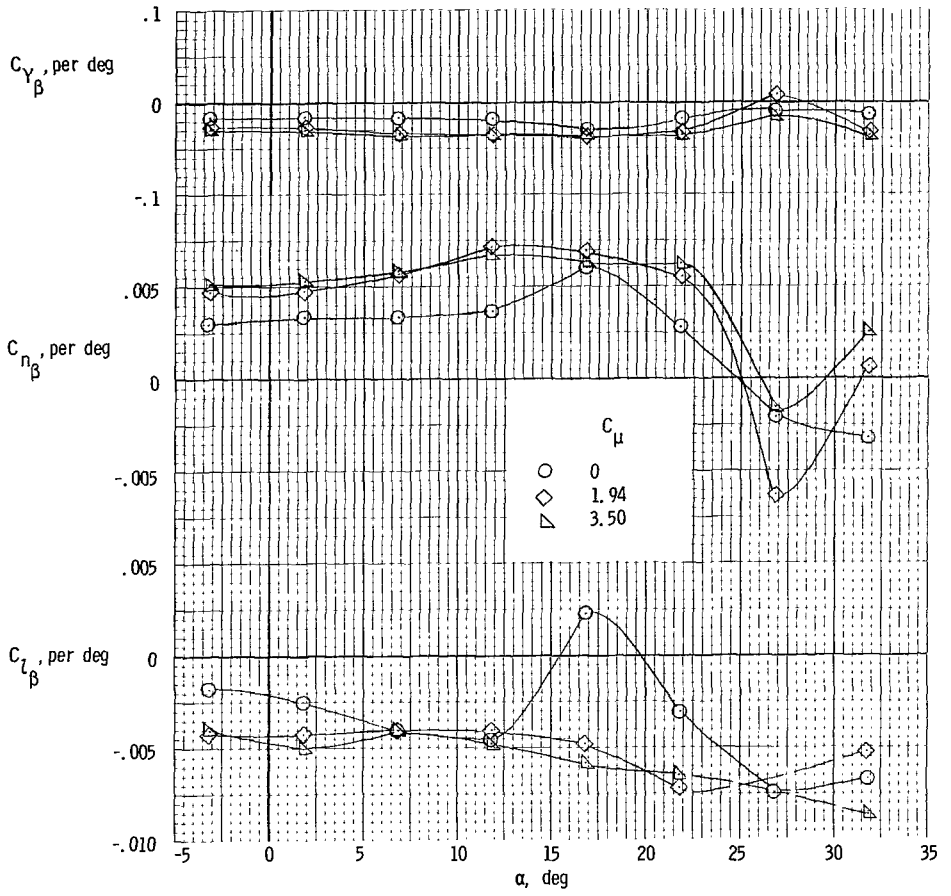

(b) $\delta_{f1}/\delta_{f2} = 20°/40°$.

Figure 17.- Continued.

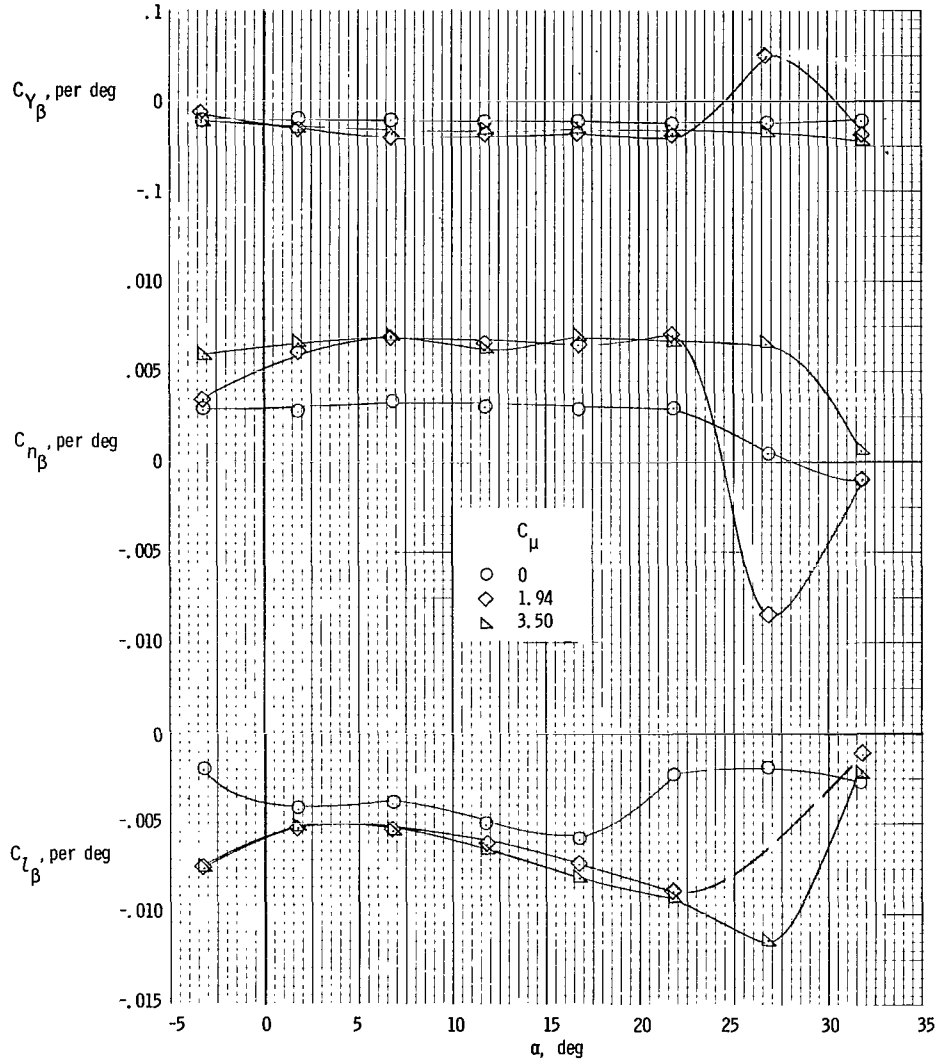

(c) $\delta_{f1}/\delta_{f2} = 30^\circ/60^\circ$.

Figure 17.- Concluded.

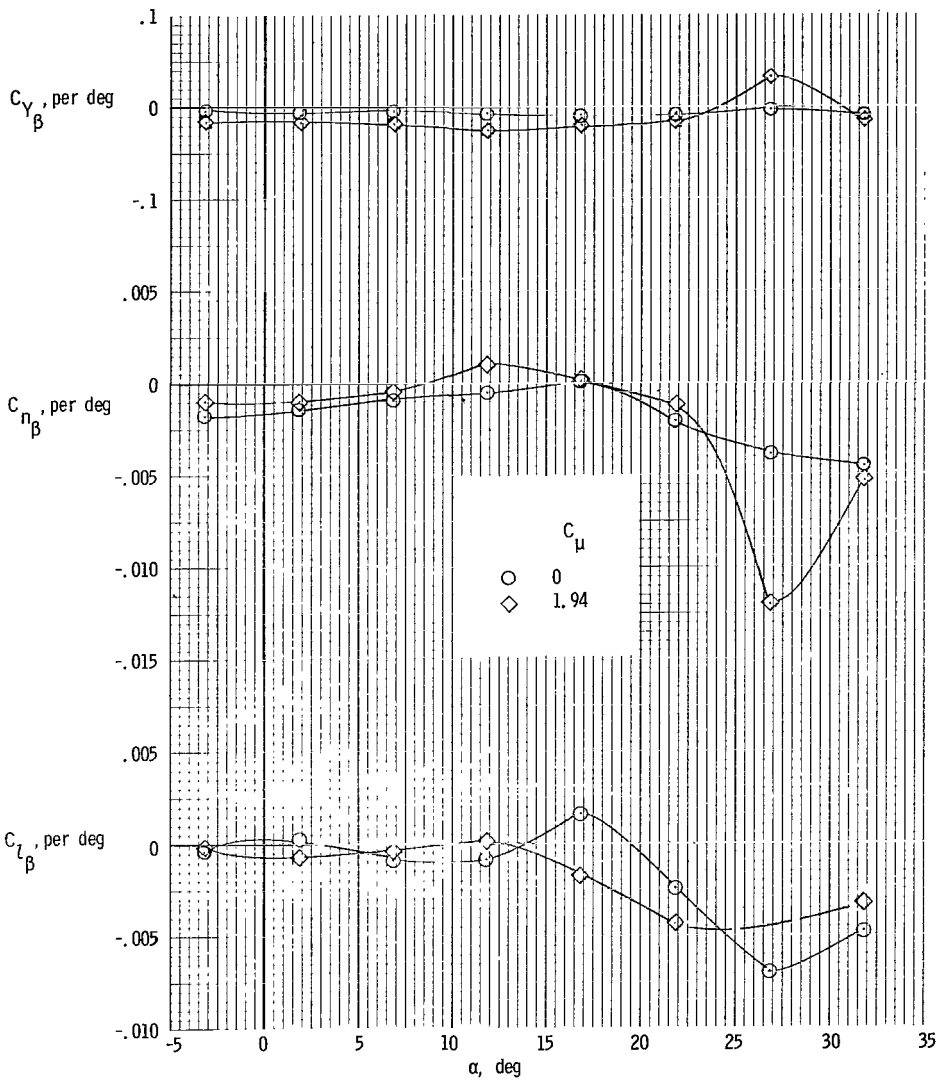

(a) $\delta_{f1}/\delta_{f2} = 20°/40°$.

Figure 18.- Lateral stability characteristics of the model with tail off.

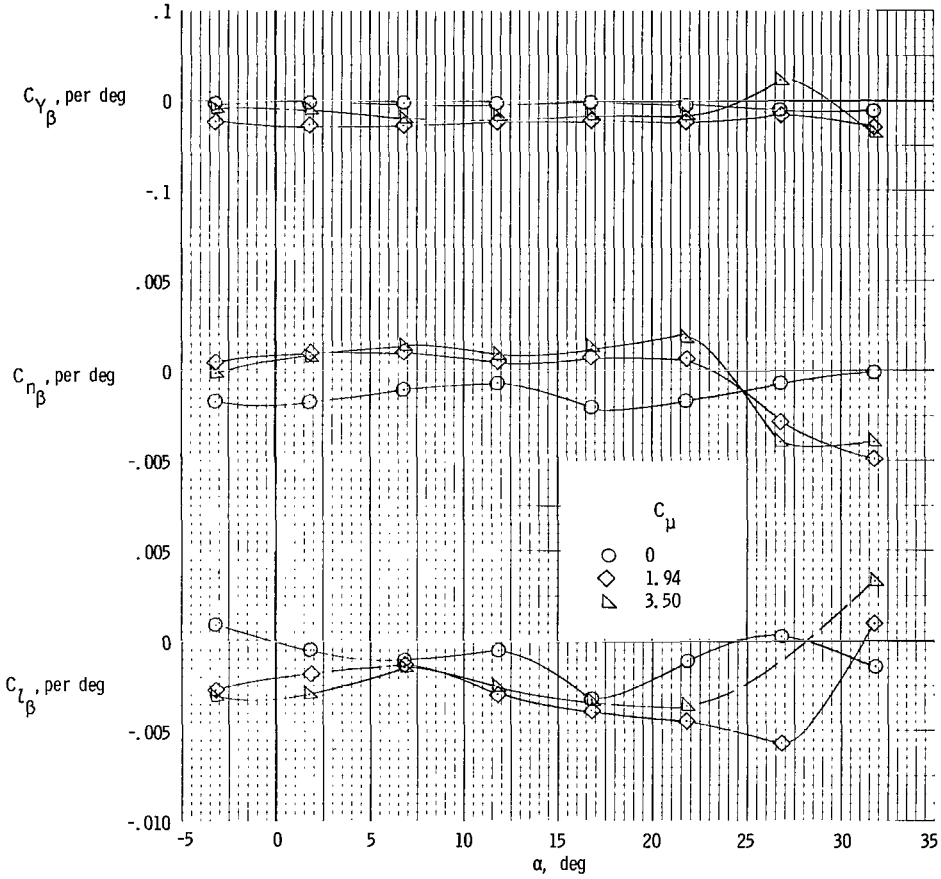

(b) $\delta_{f1}/\delta_{f2} = 30°/60°$.

Figure 18.- Concluded.

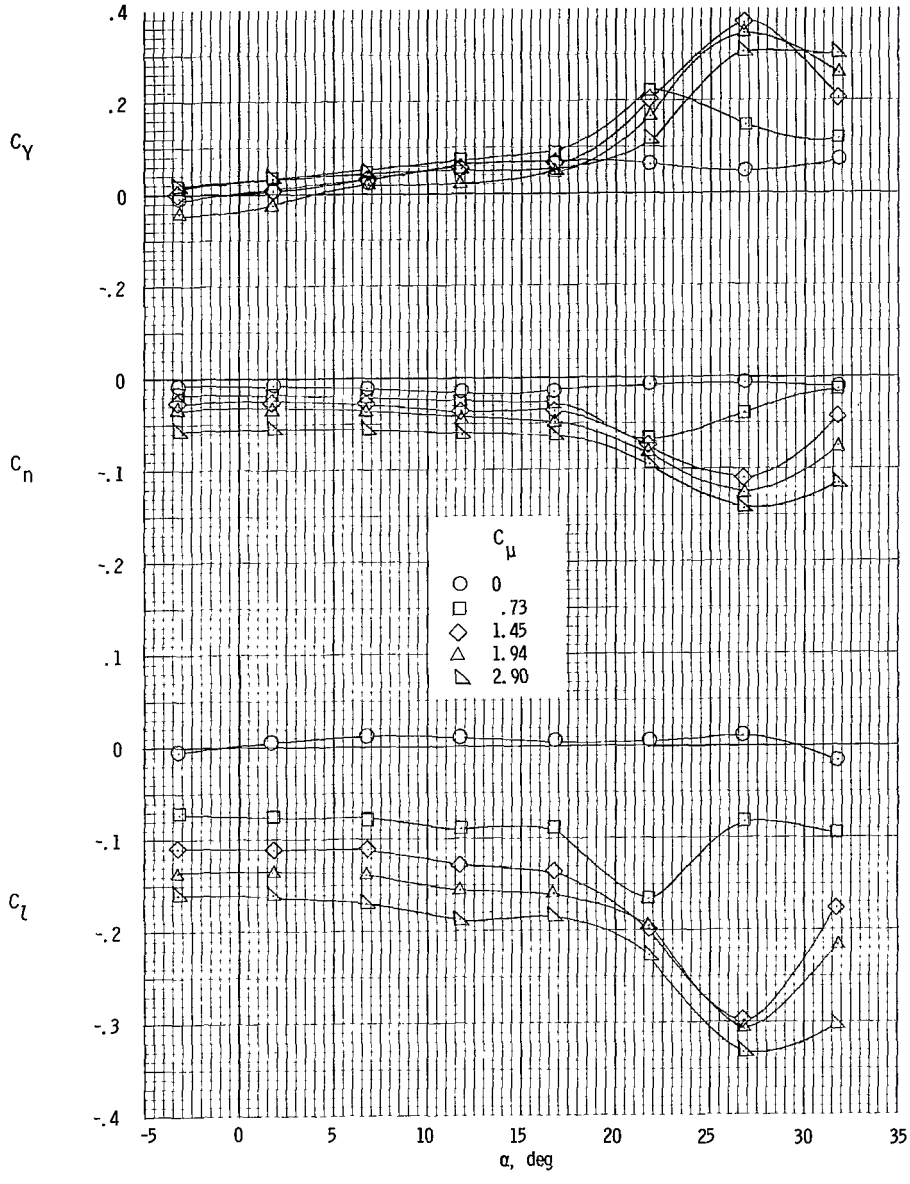

(a) Lateral characteristics; left outboard engine not operating.

Figure 19.- Effect of asymmetric thrust on lateral and longitudinal characteristics of the model with horizontal tail in high forward position and $\delta_{f1}/\delta_{f2} = 20°/40°$.

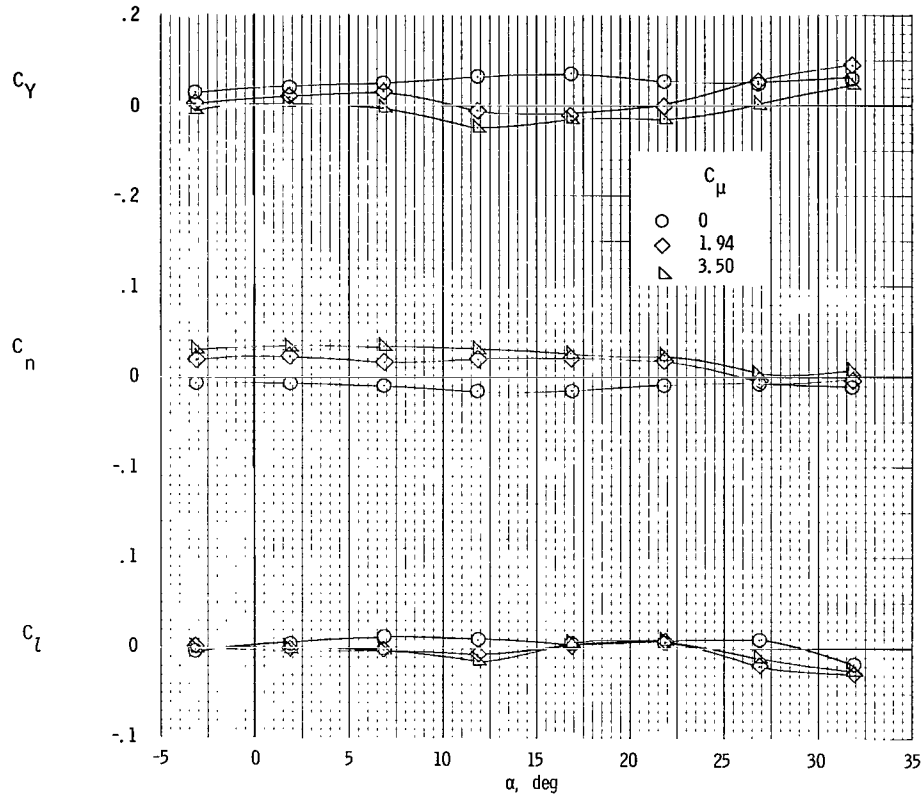

(b) Lateral characteristics; all engines operating. (For longitudinal characteristics see fig. 9(b).)

Figure 19.- Continued.

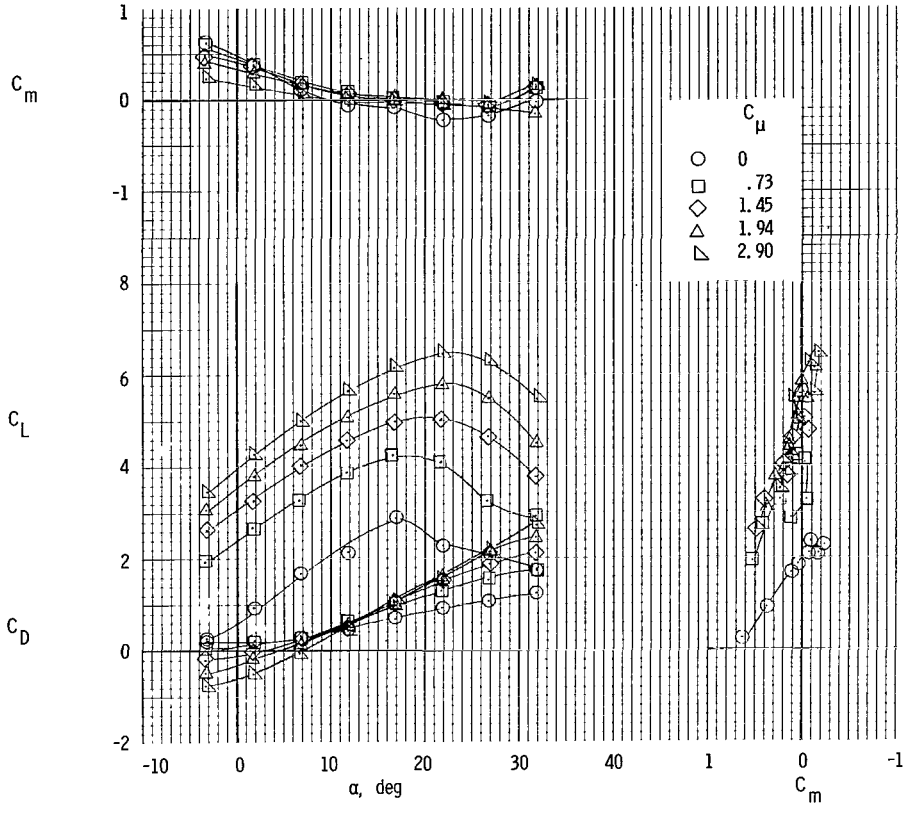

(c) Longitudinal characteristics; left outboard engine not operating.

Figure 19.- Concluded.

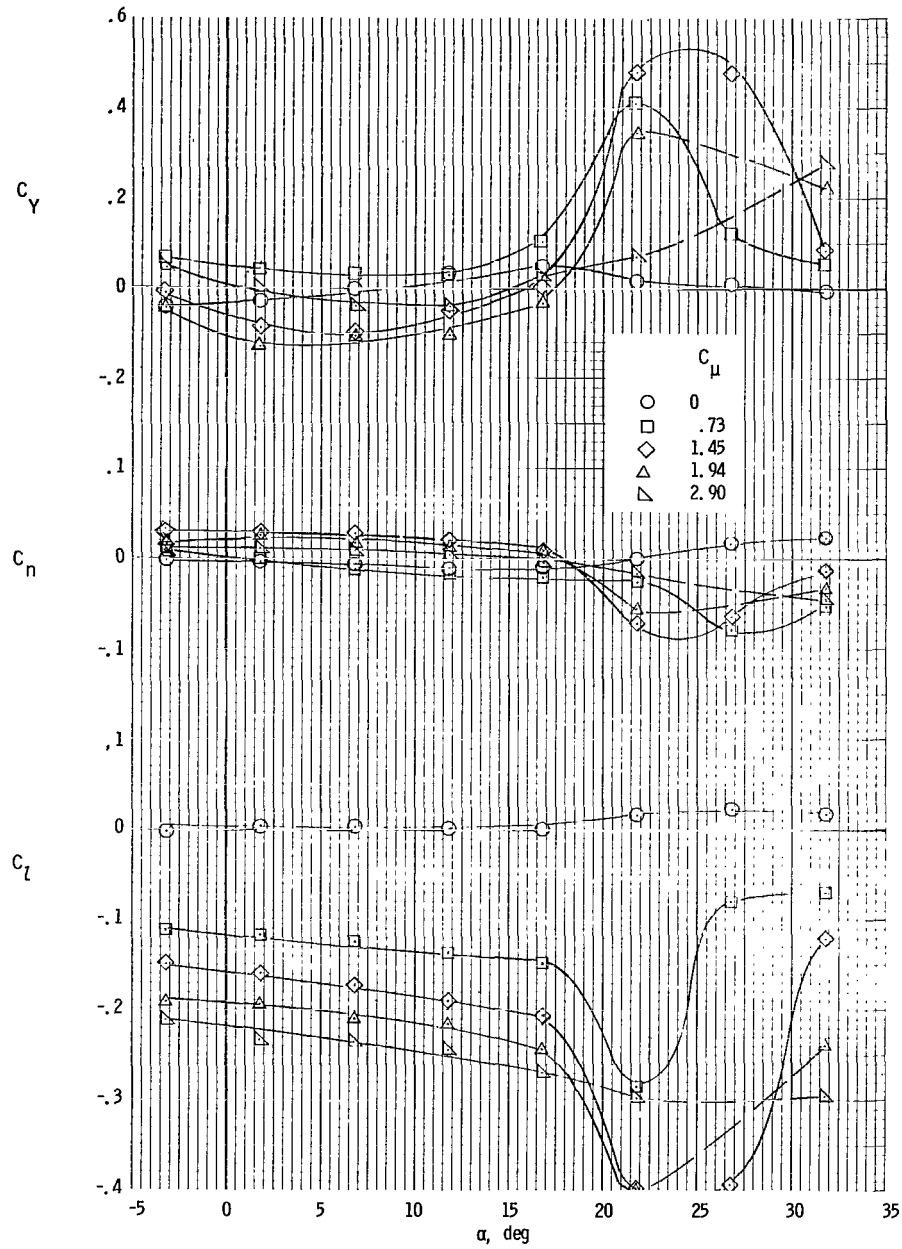

(a) Lateral characteristics; left outboard engine not operating.

Figure 20.- Effect of asymmetric thrust on lateral and longitudinal characteristics of the model with horizontal tail in high forward position and $\delta_{f1}/\delta_{f2} = 30°/60°$.

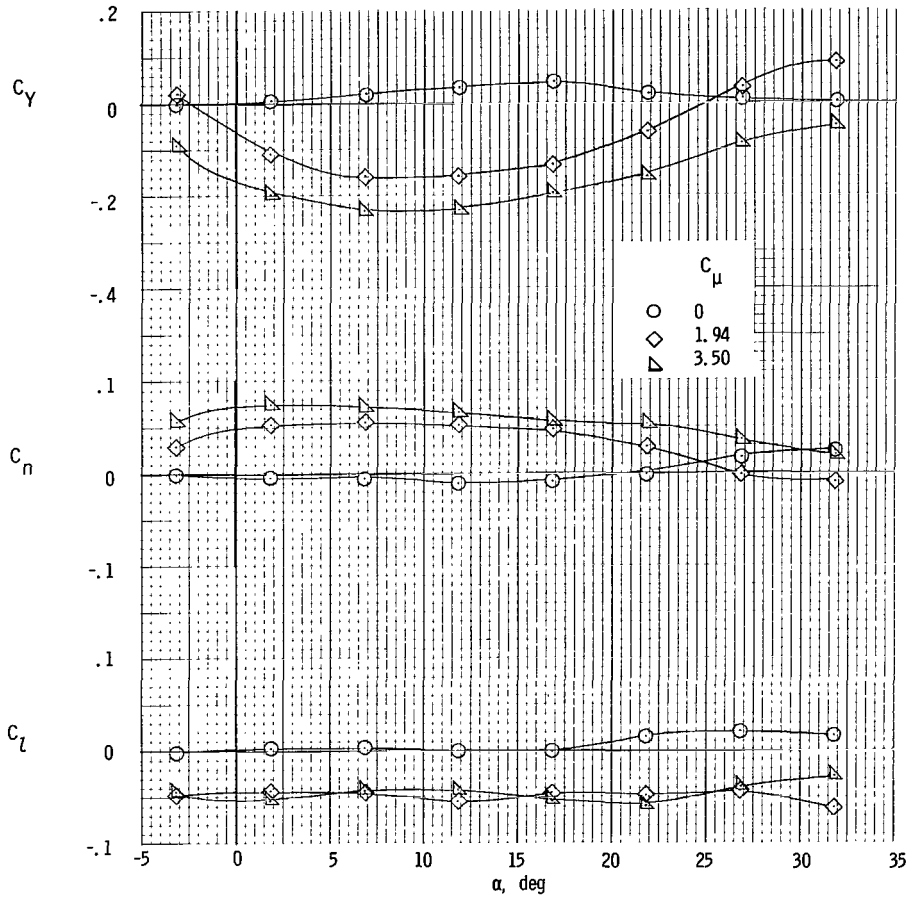

(b) Lateral characteristics; all engines operating. (For longitudinal characteristics see fig. 10(a).)

Figure 20.- Continued.

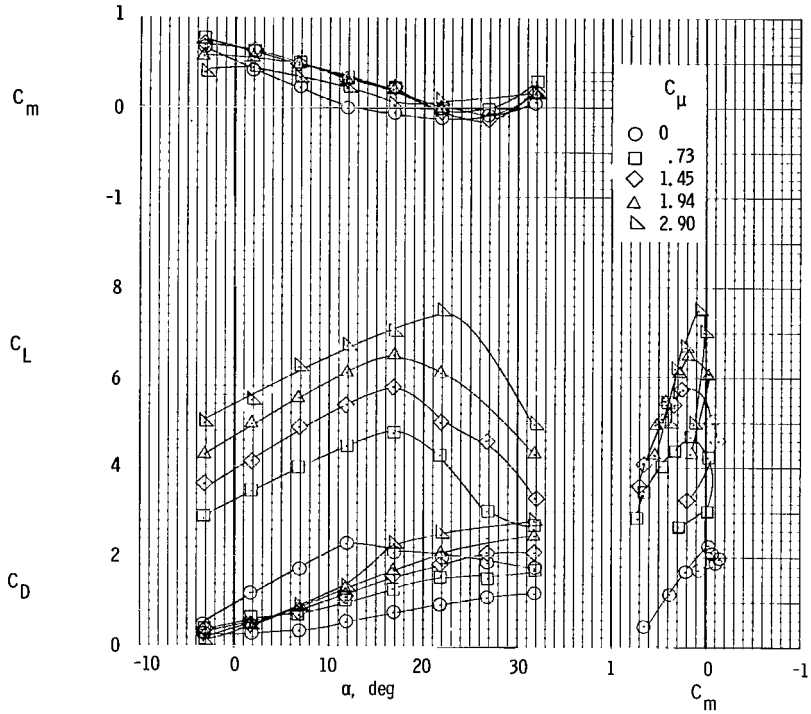

(c) Longitudinal characteristics; left outboard engine not operating.

Figure 20.- Concluded.

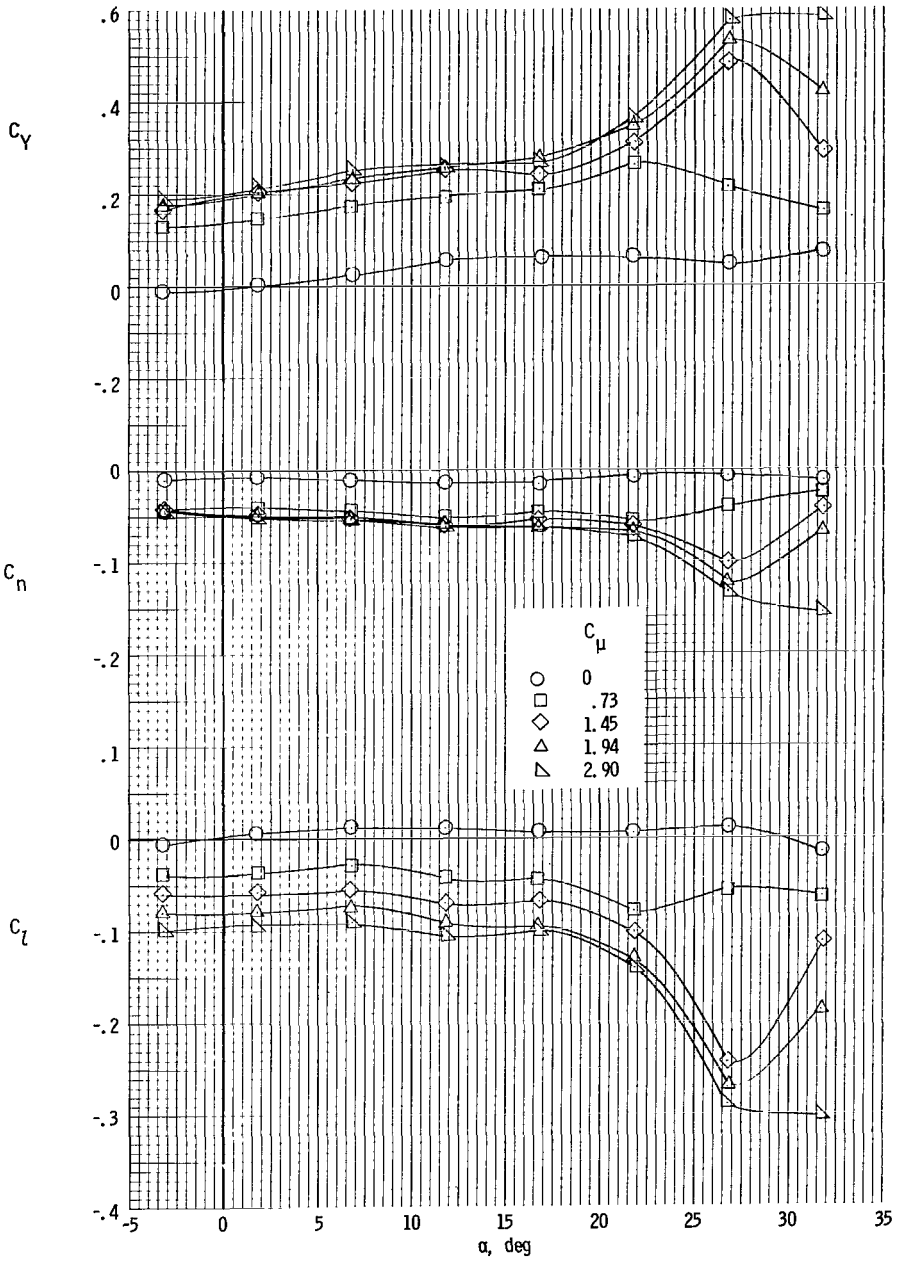

(a) Lateral characteristics.

Figure 21.- Lateral and longitudinal characteristics with left inboard engine not operating and $\delta_{f1}/\delta_{f2} = 20°/40°$.

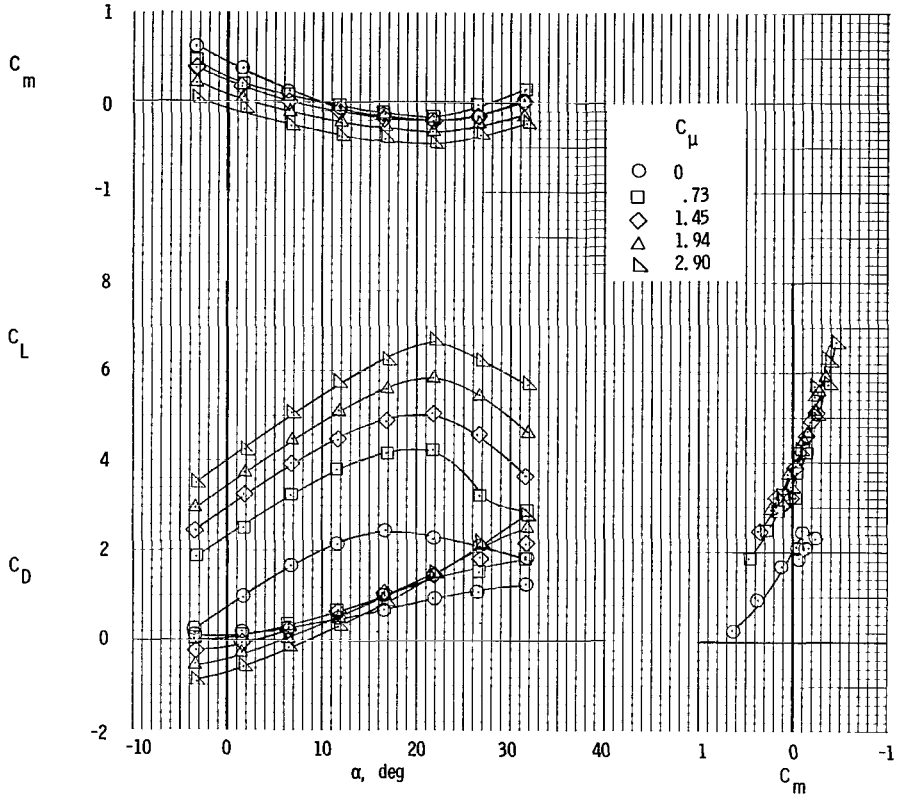

(b) Longitudinal characteristics.

Figure 21.- Concluded.

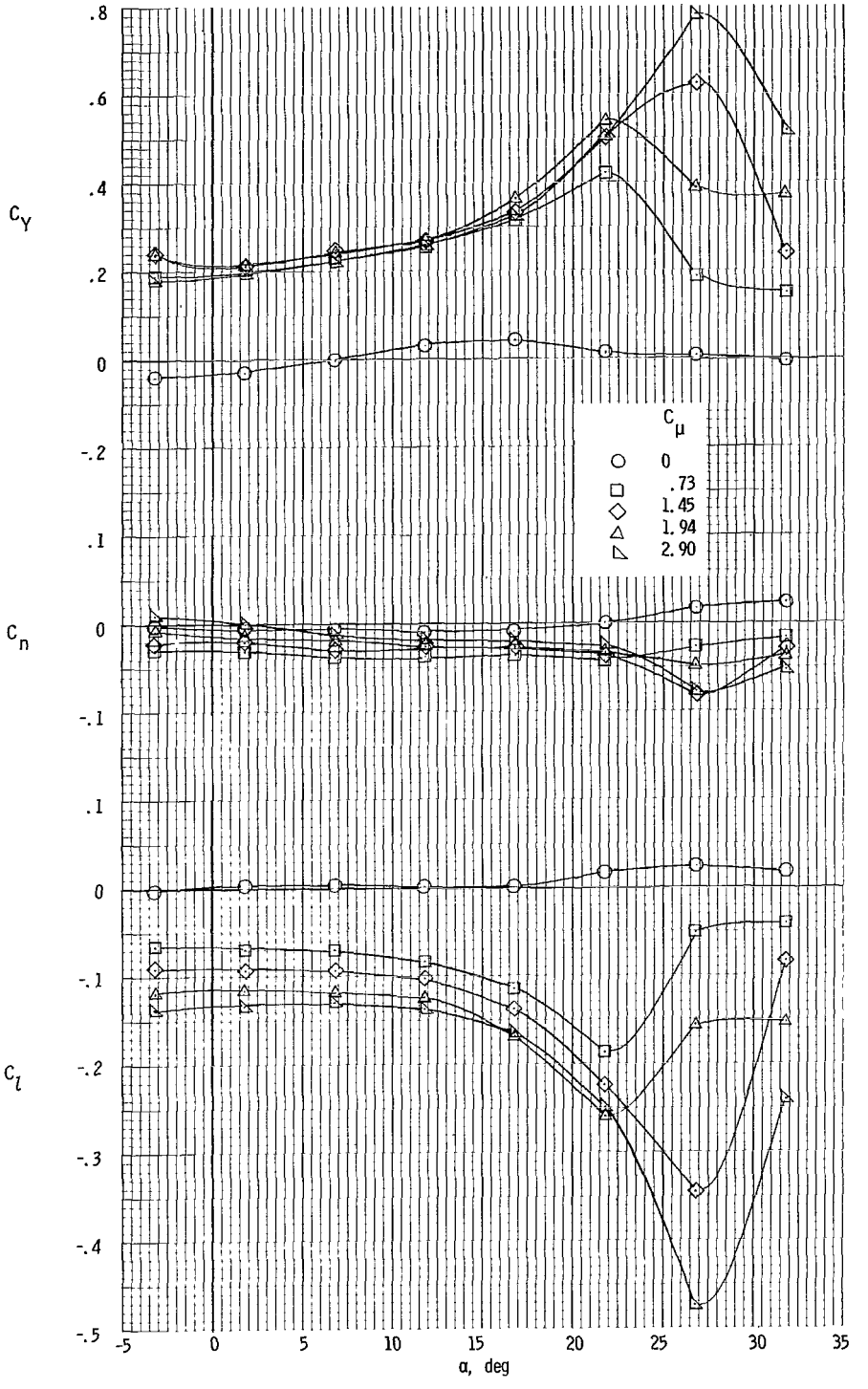

(a) Lateral characteristics.

Figure 22.- Lateral and longitudinal characteristics with left inboard engine not operating and $\delta_{f1}/\delta_{f2} = 30°/60°$.

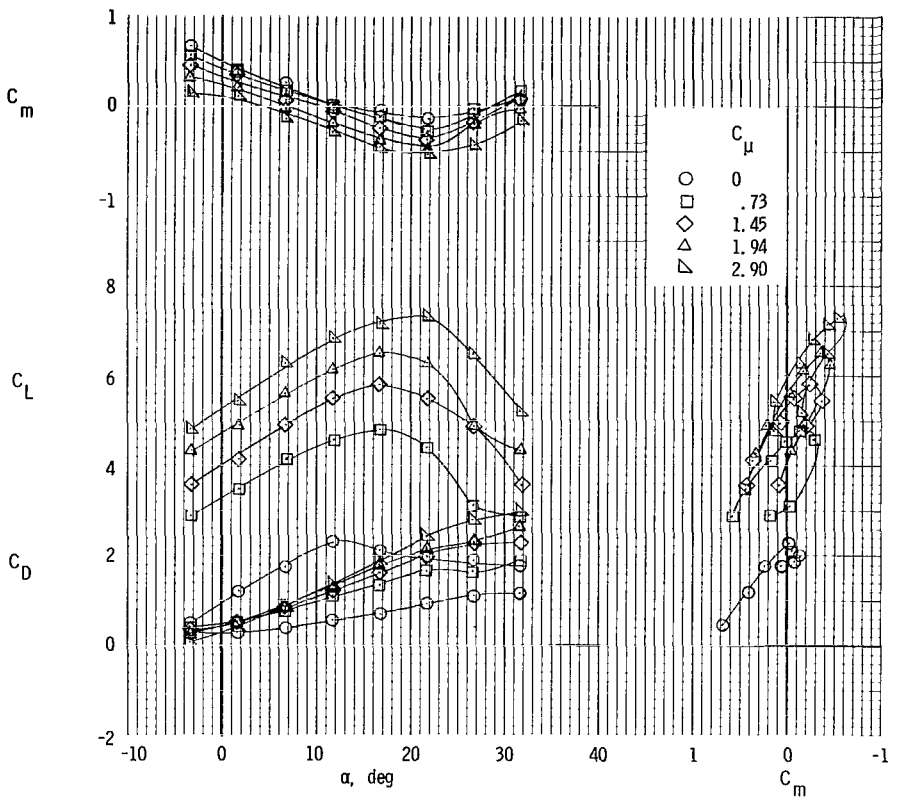

(b) Longitudinal characteristics.

Figure 22.- Concluded.

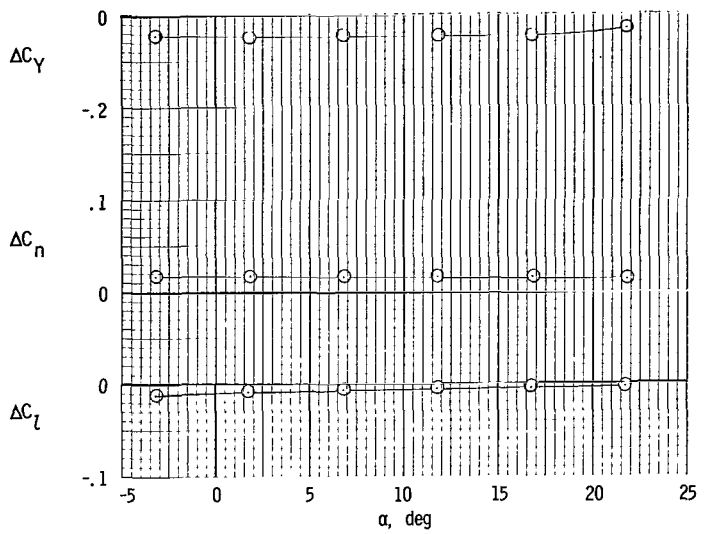

(a) $\delta_{f1}/\delta_{f2} = 0^{\circ}$; $C_{\mu} = 0$.

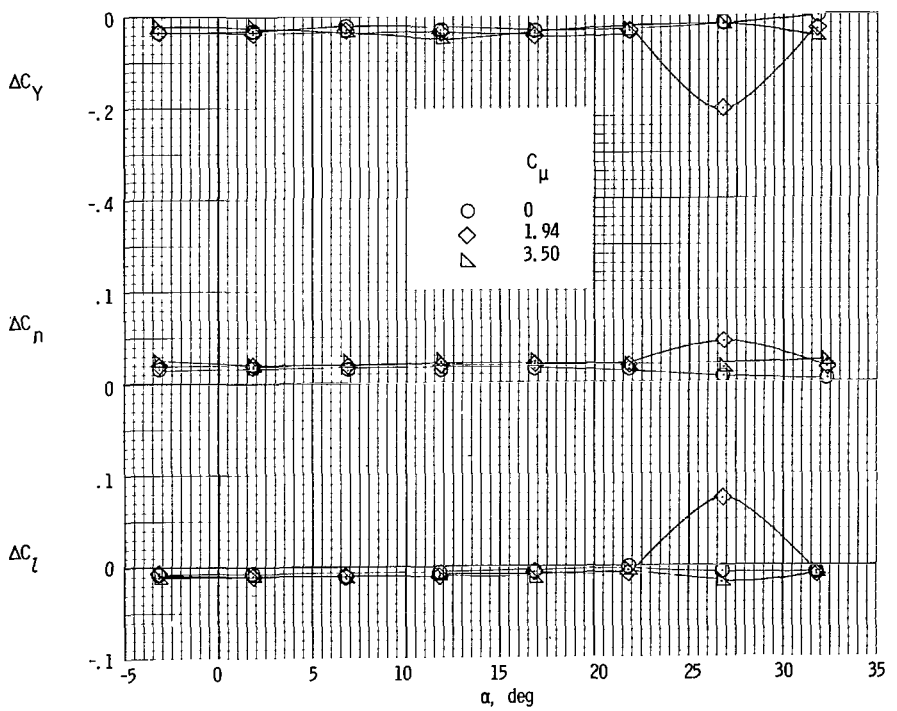

(b) $\delta_{f1}/\delta_{f2} = 20^{\circ}/40^{\circ}$.

Figure 23.- Rudder effectiveness. $\delta_r = -15^{\circ}$.

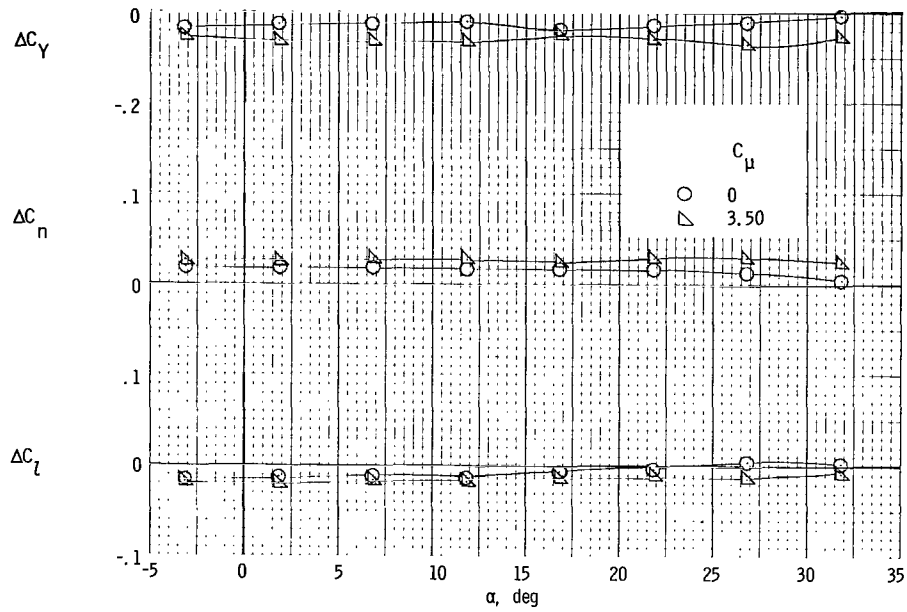

(c) $\delta_{f1}/\delta_{f2} = 30^{\circ}/60^{\circ}$.

Figure 23.- Concluded.

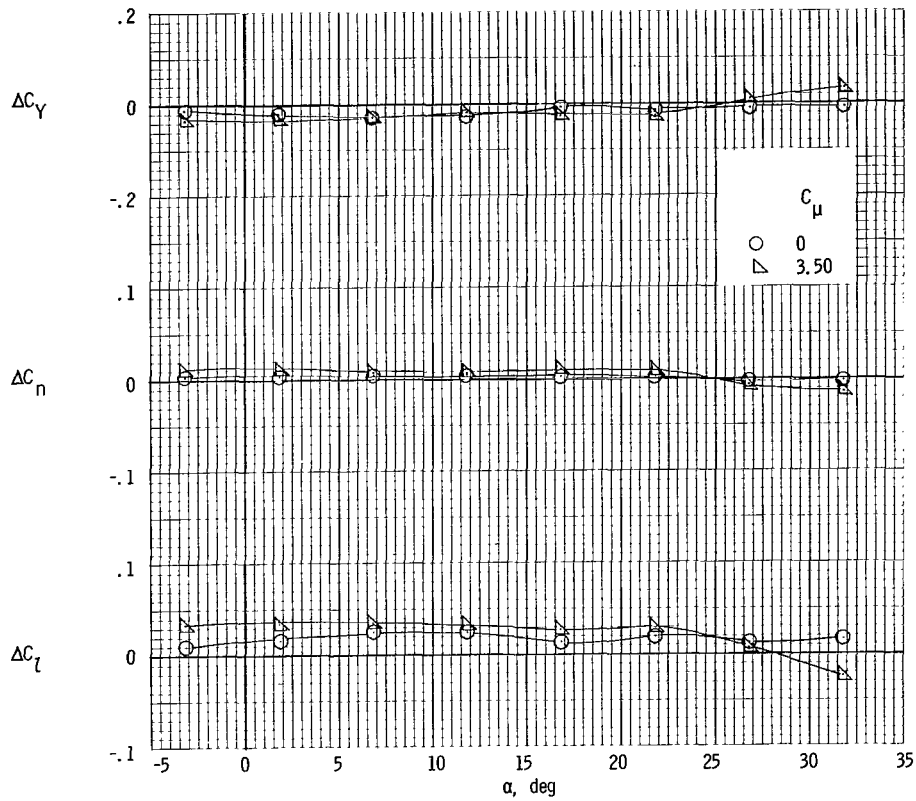

(a) $\delta_{f1}/\delta_{f2} = 20°/40°$.

Figure 24.- Aileron effectiveness. $\delta_{aL} = 15°$; $\delta_{aR} = -25°$.

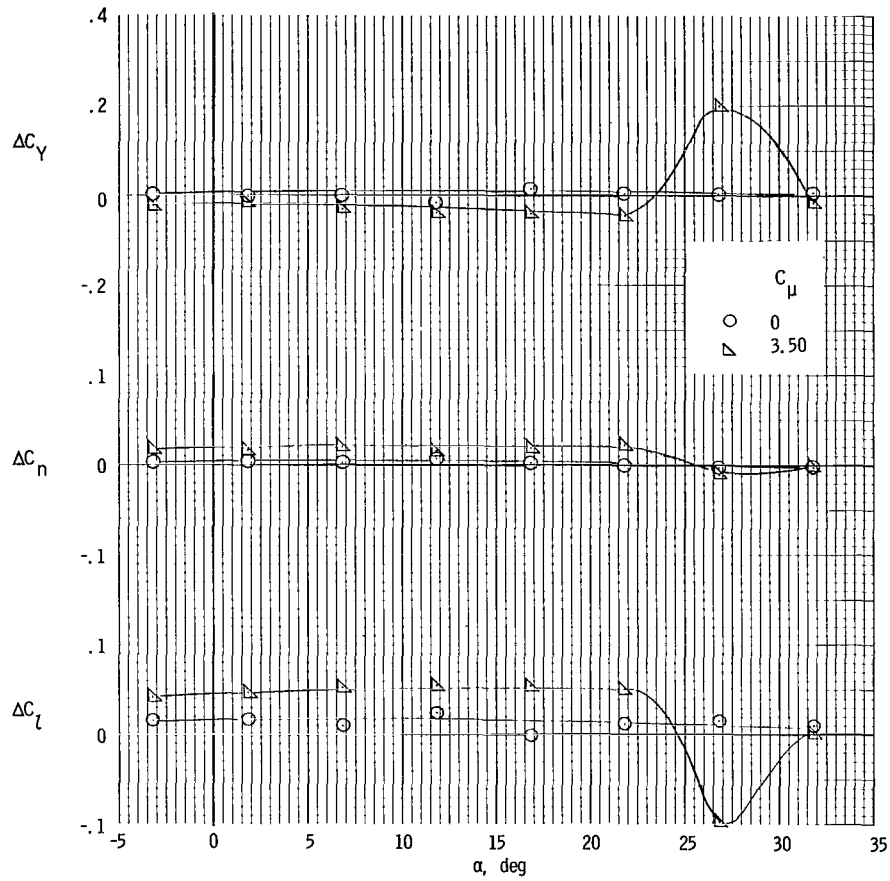

(b) $\delta_{f1}/\delta_{f2} = 30°/60°$.

Figure 24.- Concluded.

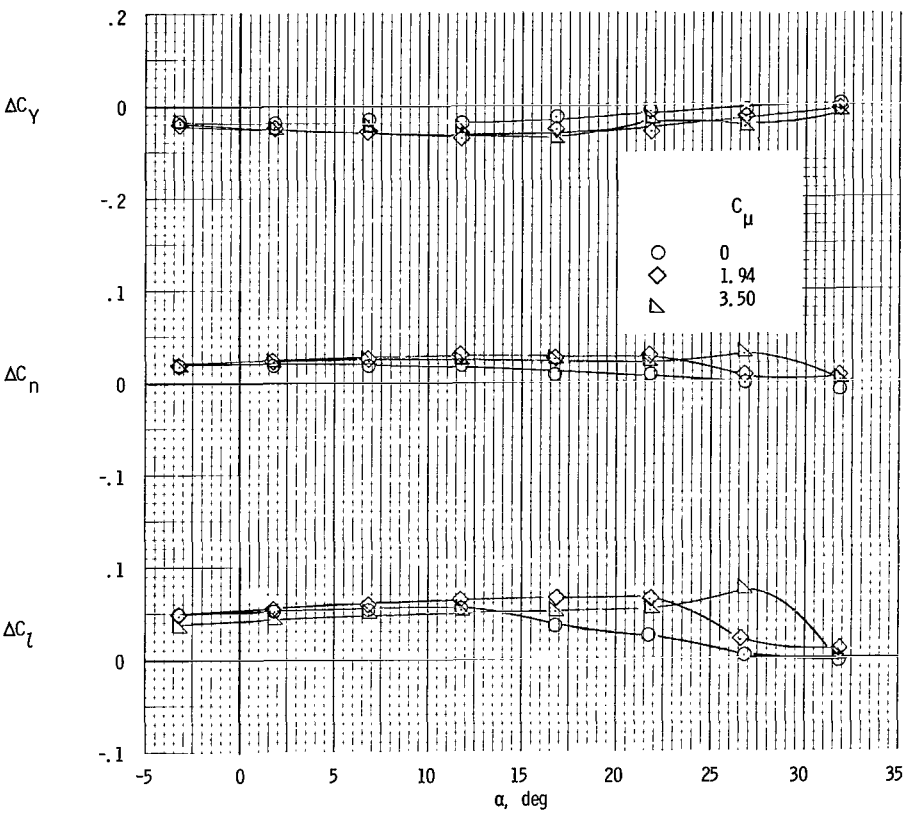

(a) $\delta_{f1}/\delta_{f2} = 20°/40°$.

Figure 25.- Effectiveness of wing spoiler deflected 60°.

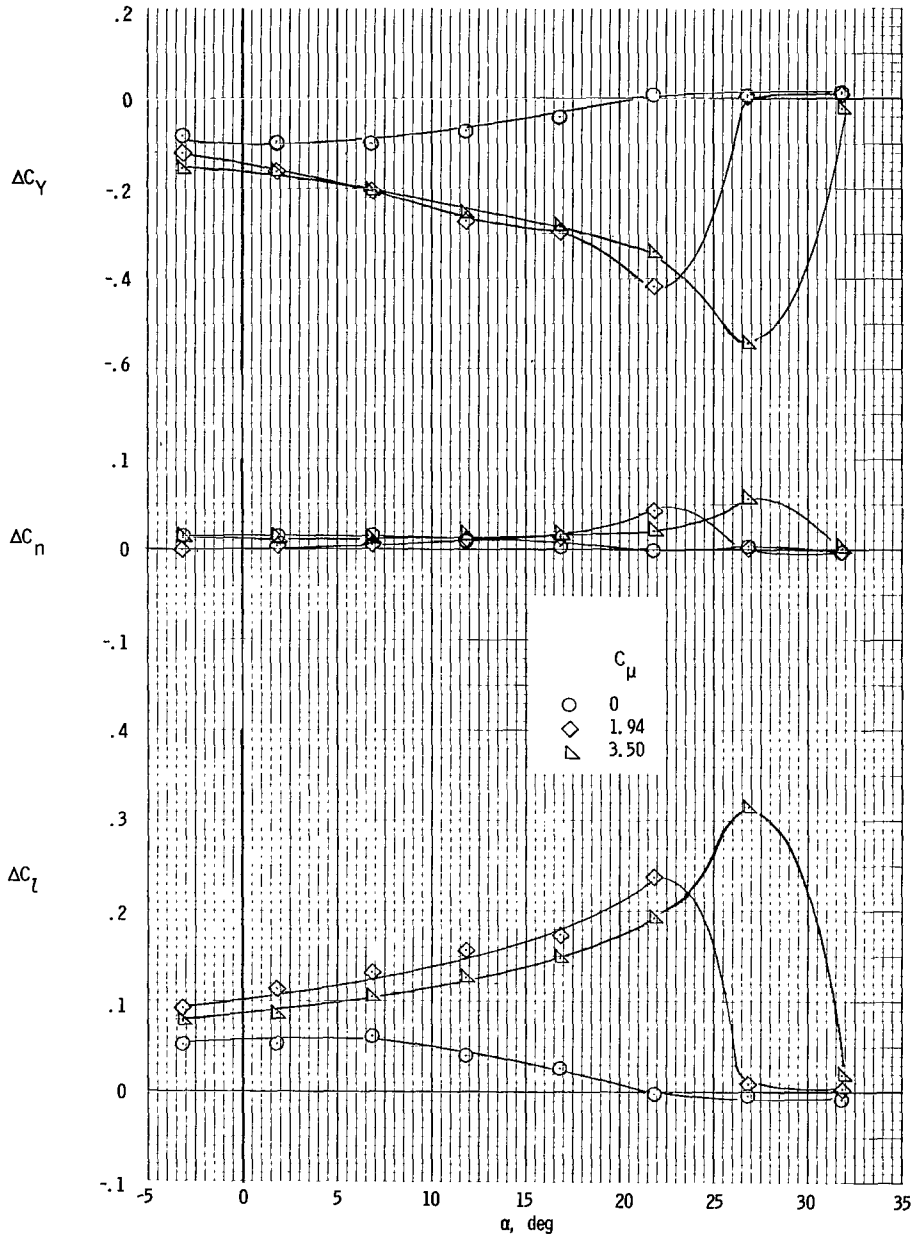

(b) $\delta_{f1}/\delta_{f2} = 30°/60°$.

Figure 25.- Concluded.

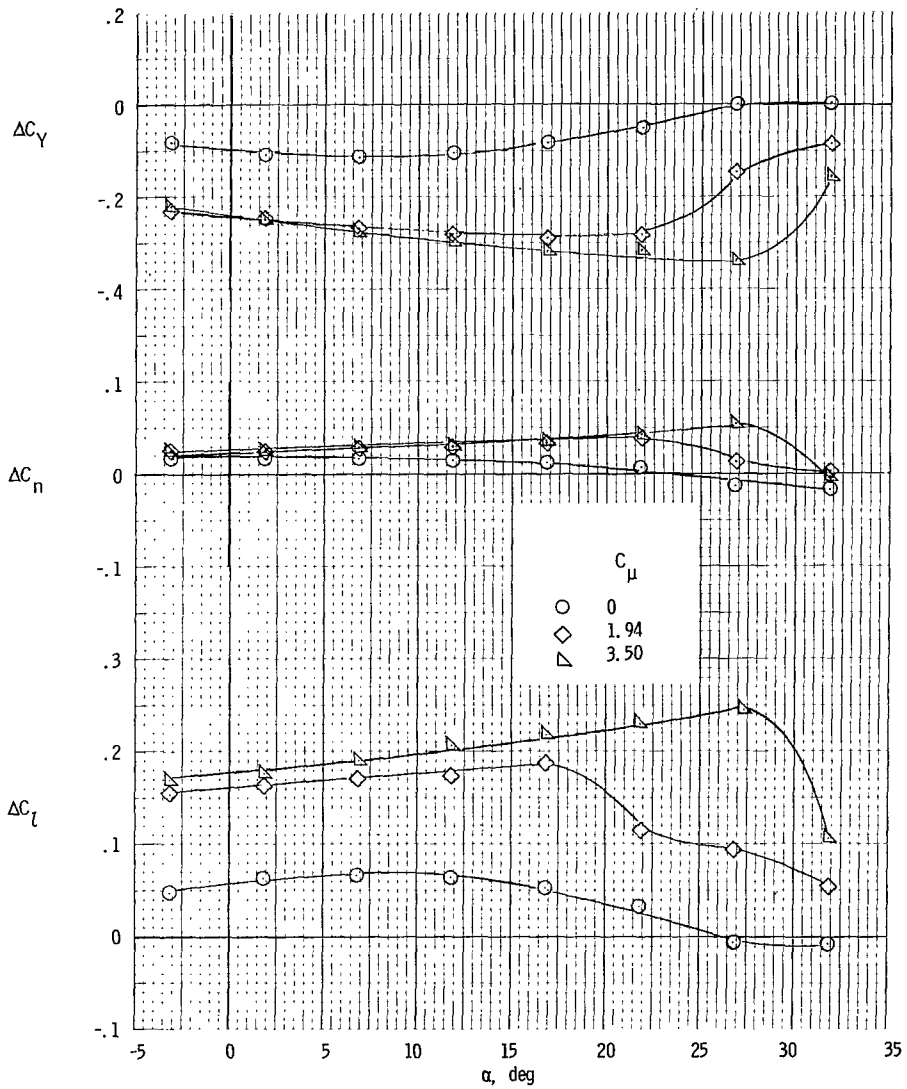

(a) $\delta_{f1}/\delta_{f2} = 20^{\circ}/40^{\circ}$.

Figure 26.- Effectiveness of wing spoiler deflected 60°; flap spoiler installed.

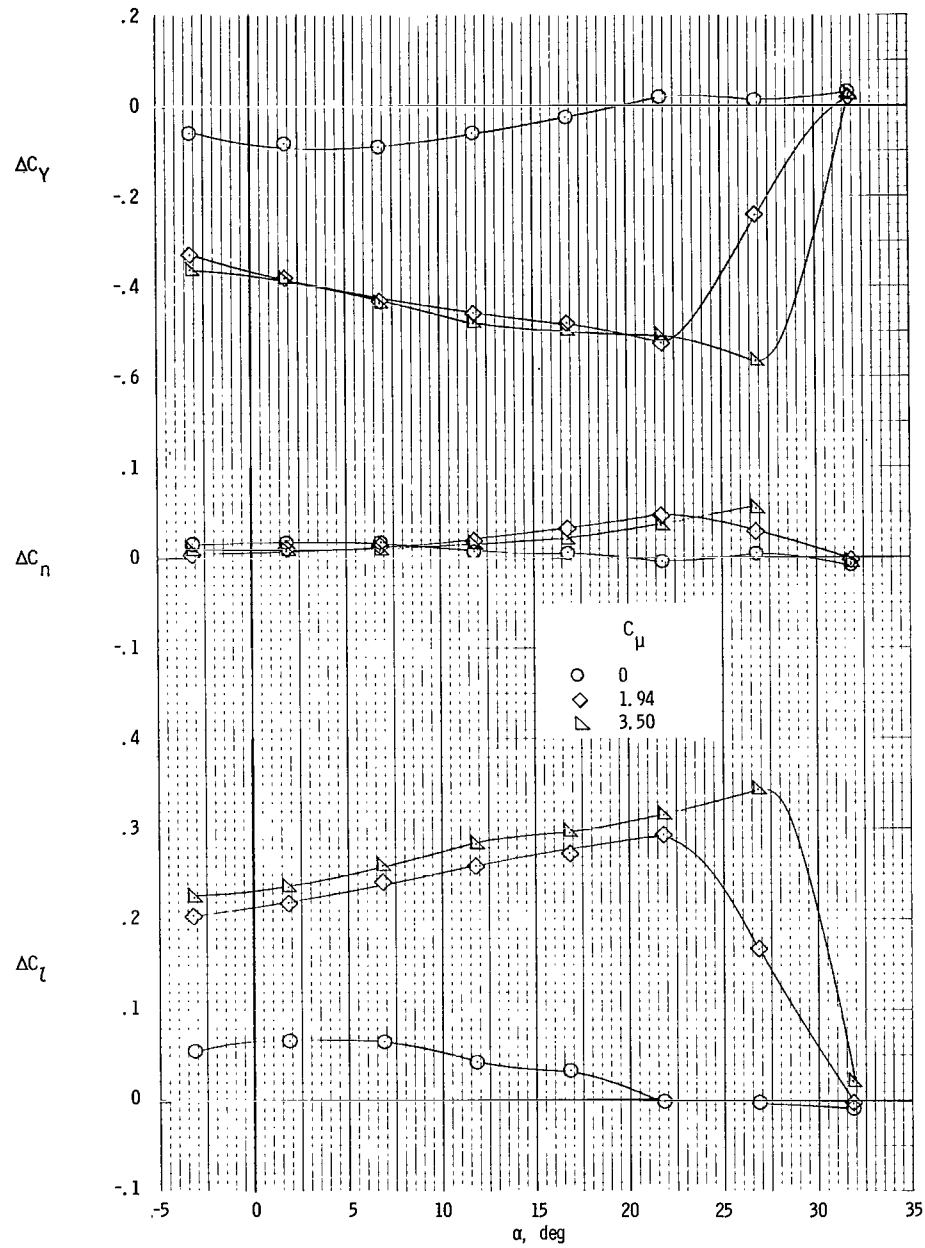

(b) $\delta_{f1}/\delta_{f2} = 30^{\circ}/60^{\circ}$.

Figure 26.- Concluded.

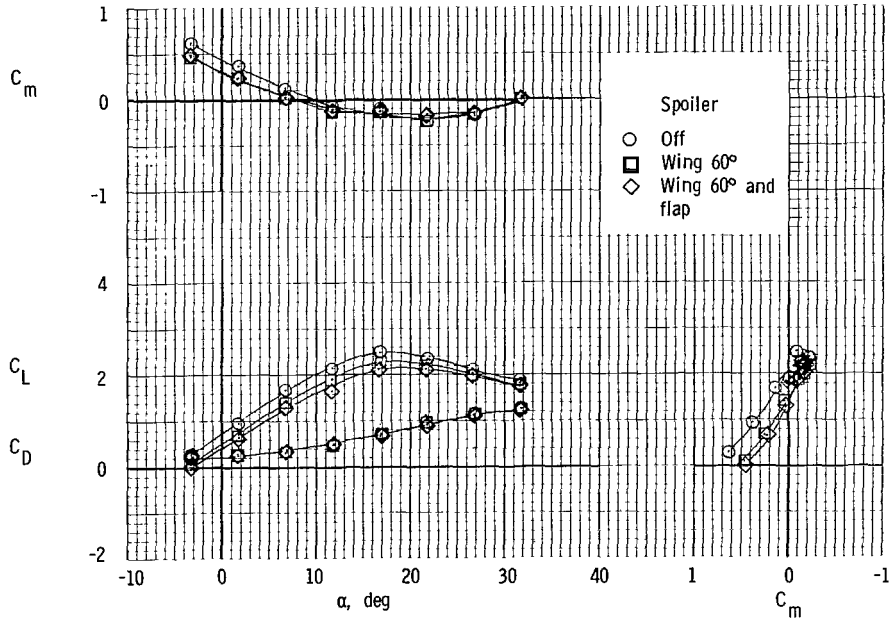

(a) $C_\mu = 0$.

Figure 27.- Effect of spoilers on longitudinal characteristics for $\delta_{f1}/\delta_{f2} = 20^\circ/40^\circ$.

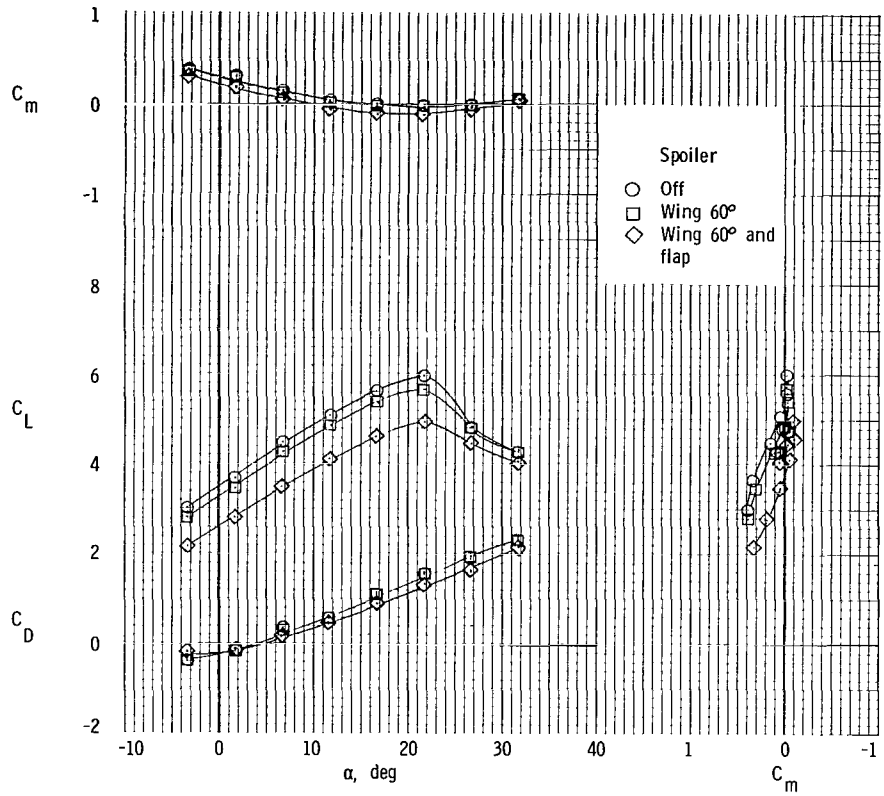

(b) C_μ = 1.94.

Figure 27.- Continued.

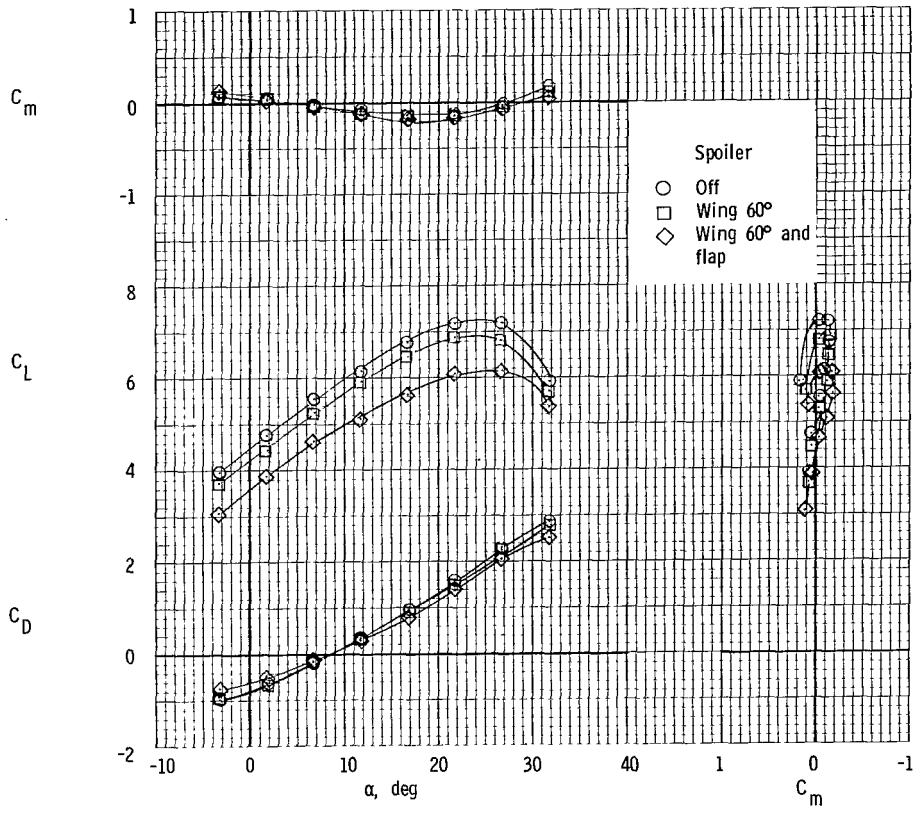

(c) $C_\mu = 3.50$.

Figure 27.- Concluded.

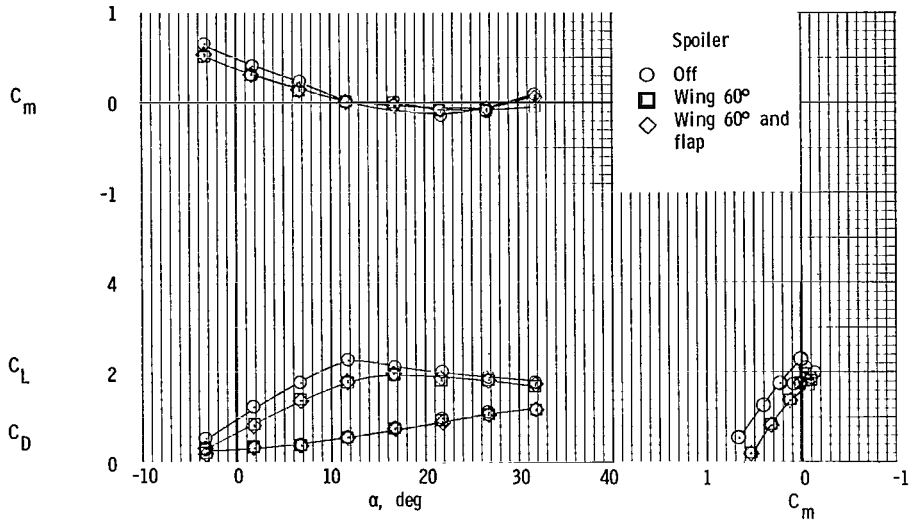

(a) $C_\mu = 0$.

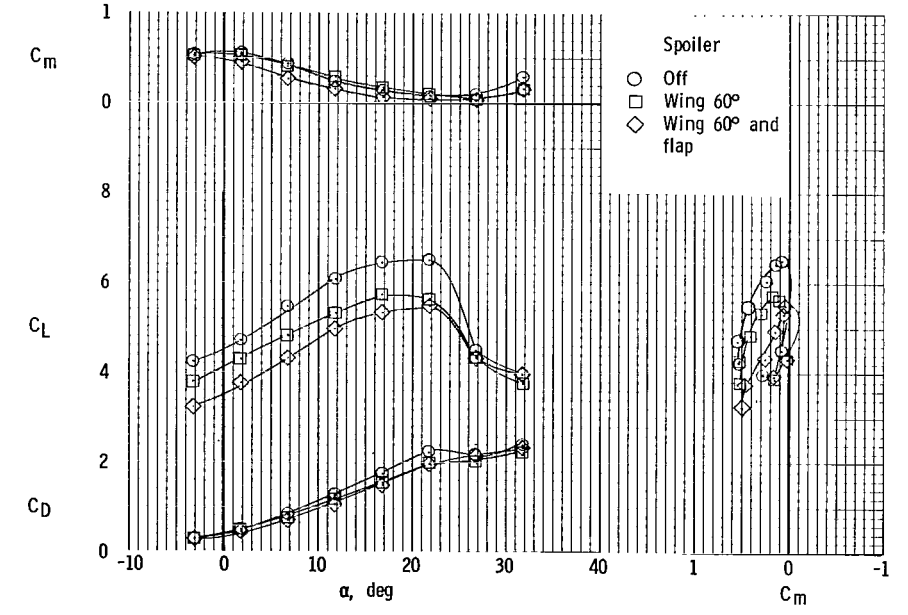

(b) $C_\mu = 1.94$.

Figure 28.- Effect of spoilers on longitudinal characteristics for $\delta_{f1}/\delta_{f2} = 30°/60°$.

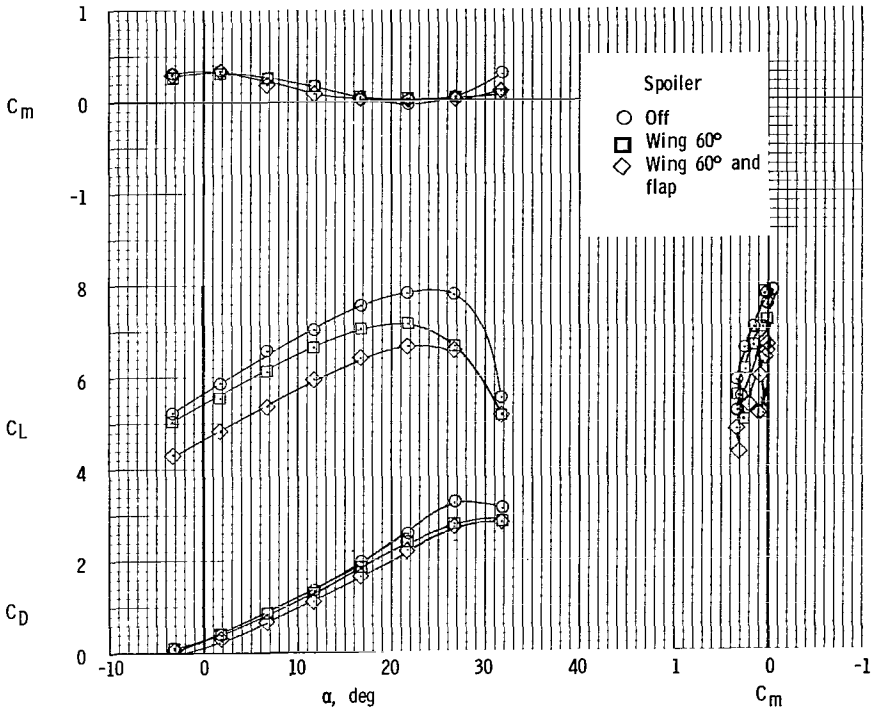

(c) $C_\mu = 3.50$.

Figure 28.- Concluded.

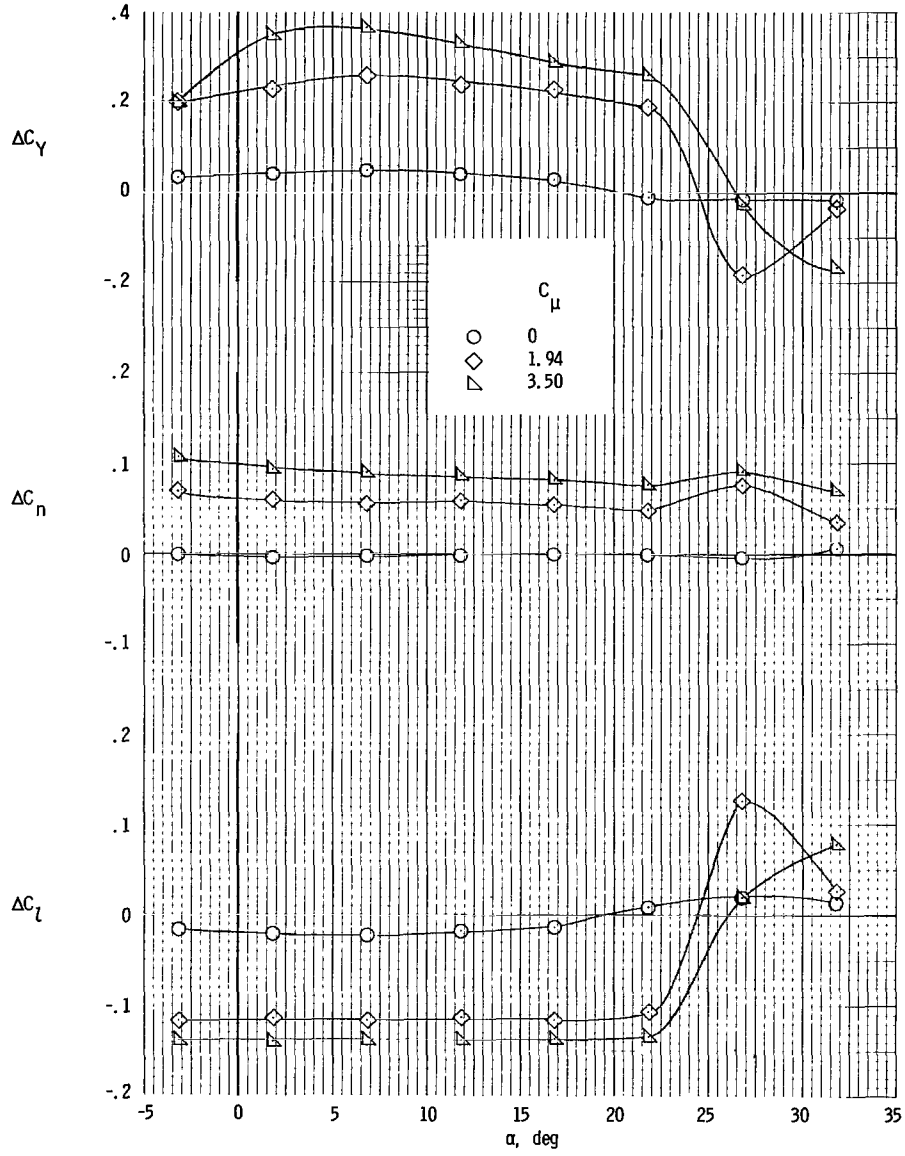

(a) Lateral characteristics.

Figure 29.- Effect of differential flap deflection on lateral and longitudinal characteristics. $\left(\delta_{f1}/\delta_{f2}\right)_L = 20°/40°$; $\left(\delta_{f1}/\delta_{f2}\right)_R = 30°/60°$.

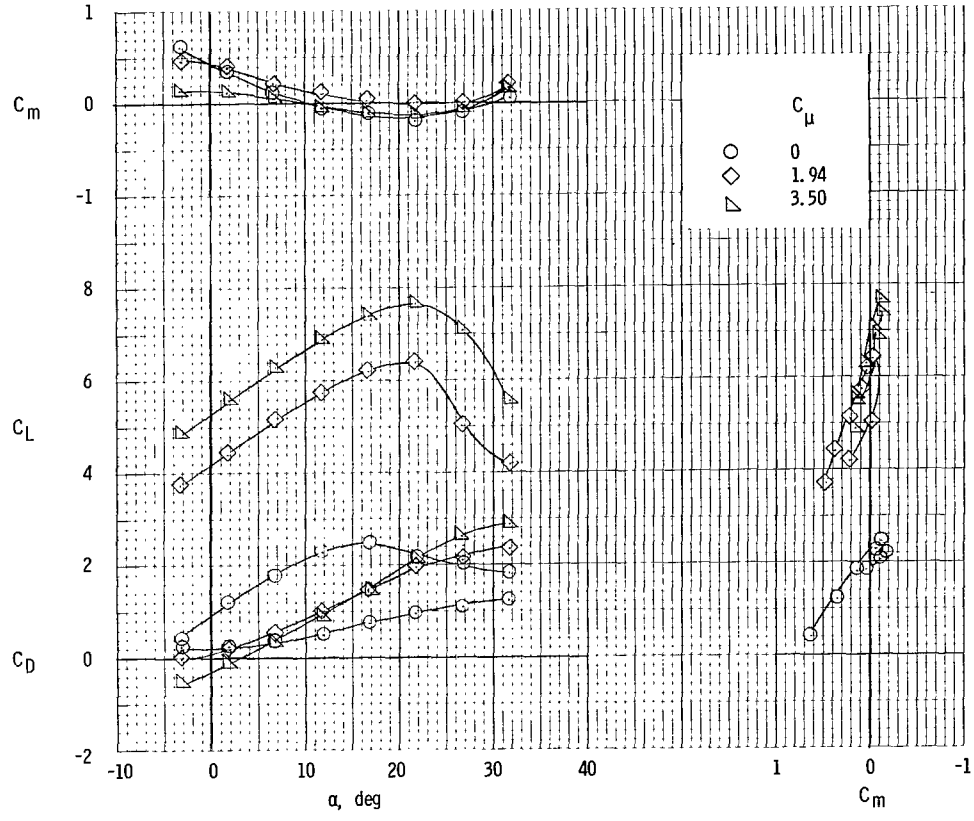

(b) Longitudinal characteristics.

Figure 29.- Concluded.

NASA-Langley, 1970 —— 26 L-7166

NATIONAL AERONAUTICS AND SPACE ADMINISTRATION
WASHINGTON, D. C. 20546

OFFICIAL BUSINESS

FIRST CLASS MAIL

POSTAGE AND FEES PAID
NATIONAL AERONAUTICS AND
SPACE ADMINISTRATION

"The aeronautical and space activities of the United States shall be conducted so as to contribute . . . to the expansion of human knowledge of phenomena in the atmosphere and space. The Administration shall provide for the widest practicable and appropriate dissemination of information concerning its activities and the results thereof."

—NATIONAL AERONAUTICS AND SPACE ACT OF 1958

NASA SCIENTIFIC AND TECHNICAL PUBLICATIONS

TECHNICAL REPORTS: Scientific and technical information considered important, complete, and a lasting contribution to existing knowledge.

TECHNICAL NOTES: Information less broad in scope but nevertheless of importance as a contribution to existing knowledge.

TECHNICAL MEMORANDUMS: Information receiving limited distribution because of preliminary data, security classification, or other reasons.

CONTRACTOR REPORTS: Scientific and technical information generated under a NASA contract or grant and considered an important contribution to existing knowledge.

TECHNICAL TRANSLATIONS: Information published in a foreign language considered to merit NASA distribution in English.

SPECIAL PUBLICATIONS: Information derived from or of value to NASA activities. Publications include conference proceedings, monographs, data compilations, handbooks, sourcebooks, and special bibliographies.

TECHNOLOGY UTILIZATION PUBLICATIONS: Information on technology used by NASA that may be of particular interest in commercial and other non-aerospace applications. Publications include Tech Briefs, Technology Utilization Reports and Notes, and Technology Surveys.

Details on the availability of these publications may be obtained from:

SCIENTIFIC AND TECHNICAL INFORMATION DIVISION

NATIONAL AERONAUTICS AND SPACE ADMINISTRATION

Washington, D.C. 20546